Deep–Sea Research I 187 (2022) 103831

Contents lists available at ScienceDirect

Deep-Sea Research Part I

journal homepage: www.elsevier.com/locate/dsri

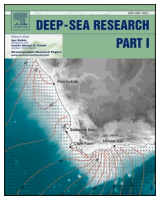

3D-Representations for studying deep-sea coral habitats in the Lacaze-Duthiers Canyon, from geological settings to individual specimens

Marie-Claire Fabri [a,*], Olivier Dugornay [c], Xavier de la Bernardie [b], Charline Guerin [c], Pierre Sanchez [a], Aurelien Arnaubec [a], Tim Autin [a], Romain Piasco [a], Pere Puig [d]

[a] Ifremer, Centre de Méditerranée, 83500, La Seyne sur Mer, France
[b] UMR 6457, SUBATECH, CNRS (IN2P3) – IMT Atlantique - Université de Nantes, 44000, Nantes, France
[c] Ifremer, Centre de Bretagne, 29280, Plouzané, France
[d] Marine Science Institute, CSIC, E-08003, Barcelona, Spain

ARTICLE INFO

Keywords:
HR Bathymetry
Photogrammetry
Micro-computed tomography
Cold-water corals
Seafloor mapping
Lophelia pertusa

ABSTRACT

The Lacaze-Duthiers Canyon is located in the western Mediterranean Sea and is long known for hosting cold-water coral colonies in the canyon head region at depths ranging from 250 to 550 m. In 2019 during the CALADU cruise, three kinds of 3D-reconstructions were applied to better understand the distribution of coral colonies, their habitat and their skeleton morphologies.

The canyon's flanks were mapped using a hull-mounted echosounder and an ROV multibeam echosounder. Digital terrain models were built with resolutions of 5 and 1 m and examined in three dimensions. ROV bathymetric data collected on the canyon's flanks made it possible to highlight a series of sub-parallel structures identified as lithified sedimentary strata along which coral colonies grow.

Coral assemblages were explored at four locations and photographic images were assembled using structure from motion techniques to build photogrammetric models. Coral assemblages reconstructed in 3D enabled geo-localizing and recreating coral colonies on 16 models over a total area of 4370 m^2. Two colonial species, *Madrepora oculata* and *Desmophyllum pertusum* were plotted and reported on bathymetric models to interpret their location at the scale of the canyon. The coordinates and depth of the colonies were used to calculate the vertical distribution (limited to our small bathymetric exploration, between 339 and 214 m depth) and density of populations (up to 4.3 colonies per m^2). The spatial coverage of the 16 assemblages measured between 100 and 600 m^2 each. The sizes of the colonies were measured to analyze the population structures of both species (mean sizes of 28 cm for *D. pertusum* and 18 cm for *M. oculata*, maximum sizes 1 m and 0.5 m, respectively, bushes 2.5 m long). In addition, lost fishing gears were quantified, longlines measured and their densities calculated (0.16 m/m^2, up to 0.30 m/m^2). An area with exuberant orange colonies of *D. pertusum* was discovered for the first time in the Lacaze-Duthiers Canyon.

Five deep-sea scleractinian species were collected and micro-tomographic scans computed to view their intrinsic skeleton organization. Micro-CT scans of *M. oculata*, *D. pertusum*, *Desmophyllum dianthus*, *Caryophyllia smithii*, and *Dendrophyllia cornigera* enabled longitudinal and transversal cuts, highlighting morphological criteria for species identification and the multidirectional examination of specimens. We observed a thin canal connecting calices along the axis of *D. pertusum* colonies, and separate calices along the axis of *M. oculata* colonies.

1. Introduction

The oceans have long remained an unknown world and man has always dreamed of being able to empty them to observe the reliefs of their beds. The General Bathymetric Chart of the Oceans (GEBCO) provides publicly-available bathymetric data on the world's oceans. It incorporates data derived from both single-beam and modern high resolution Multibeam Echo-Sounders (MBES), superimposed on a base derived from satellite altimetry (Mayer et al., 2018). For remote areas, altimetric satellites were used to measure the height of the ocean's surface, which is affected by, among other things, the gravitational effects of topographic features on the seafloor (Wolfl et al., 2019). Thus,

* Corresponding author.
E-mail address: Marie.Claire.Fabri@ifremer.fr (M.-C. Fabri).

https://doi.org/10.1016/j.dsr.2022.103831
Received 31 August 2021; Received in revised form 26 June 2022; Accepted 27 June 2022
Available online 30 June 2022

large geomorphological features of the ocean floor were revealed by such topographic maps and then bathymetric precision on oceanic ridges, continental margins, seamounts and canyons helped to improve understanding of their geological evolution. At the European scale, EMODnet (www.emodnet.eu) also provides free bathymetric information, mainly oriented towards European waters. However, better spatial resolutions are needed to perform detailed geomorphometric analyses (Lurton, 1998).

In the western Mediterranean, the Gulf of Lion and its canyon system have been intensively surveyed and mapped (Loubrieu and Satra, 2010) to better understand the morphodynamics of the continental margin (Berné et al., 1999; Baztan et al., 2005; Berné and Gorini, 2005; Sultan et al., 2007; Dennielou et al., 2009). The Gulf of Lion drains alluvium and particles from the Rhone river, the 2nd largest river flowing into the Mediterranean Sea after the Nile (Durrieu de Madron et al., 1999, 2000; Palanques et al., 2006). It is also the location of dense water formation during wintertime and where dense shelf water cascading overflows occur (Durrieu de Madron et al., 2005; Canals et al., 2006; Palanques et al., 2012). The steepest parts of canyon flanks are often exposed to these intense cascading currents, providing ideal habitats for sessile fauna dependent on currents for food intake. Long inaccessible to humans, these harsh environments gradually came to light with the arrival of manned submersibles, Remote Operated Vehicles (ROV) and Autonomous Underwater Vehicles (AUV). MBES installed on oceanographic vessels generate accurate maps that provide valuable information of the seafloor morphology, but when MBES are installed on underwater robotic vehicles, it is possible to get closer to the bottom and thus to increase the resolution of bathymetric maps and even detect the presence of coral mounds and coral reefs (Huvenne et al., 2011; Savini et al., 2014; Fabri et al., 2017; Robert et al., 2017). Three-dimensional representations of under-water landscapes make it possible to better understand the drivers of ecosystem distribution, like hard substrates, vertical walls and even overhanging habitats (Lim et al., 2021).

Marine habitats are being studied by underwater vehicles in an increasingly methodical way, and habitat mapping is becoming an essential tool not only for scientists but also for habitat conservation and the sustainable use of marine resources (Buhl-Mortensen et al., 2015). Advances in map resolution and in the accuracy of underwater-vehicle navigation (Raugel et al., 2019), combined with algorithms capable of using the position of under-water vehicle and camera settings, now allow accurate spatial positioning. The assemblage of several images of the same object allows its reconstruction in 3 dimensions. The final model is a representation of a marine habitat, perfectly scaled and located in space (Arnaubec et al., 2015). These photogrammetric models allow ecologists to measure various parameters useful for understanding benthic populations and environments. They are particularly useful when a 2-dimensional map does not provide a good representation of habitat complexity (Fabri et al., 2019; Price et al., 2019).

Photogrammetric models are useful to create an overview of a marine ecosystem, allowing measurements of surfaces and sizes, and giving access to quantitative parameters. The necessity to quantify ecosystem status is becoming an urgent need with the recent regulations put in place in European waters. The Marine Strategy Framework Directive (MFSD) issued in June 2008 was adopted to achieve good environmental status in the EU's marine waters and to protect resources of socioeconomic interest (European Commission, 2008). The MFSD also includes deep-sea waters, the seabed and the subseafloor; however, at present it has mostly focused on shallow coastal habitats (Danovaro et al., 2020; Orejas et al., 2020). Descriptors requested by the MFSD to evaluate the state of benthic ecosystems are based on the surface area and percentage of impacted areas. Therefore, the use of photogrammetric models, a non-intrusive method allowing the reconstruction of scaled and georeferenced parts of the seafloor, is becoming more and more popular for the assessment of vulnerable ecosystem statuses. Our study is an attempt to apply this method for evaluating the status of cold-water corals in the Lacaze-Duthiers Canyon.

Images taken by underwater vehicles make it possible to recognize and quantify the different species that make up an ecosystem. Some of these many species are called "ecosystem engineers" because of their ability to build 3D habitats for other species (Buhl-Mortensen et al., 2010). To better understand how these species are constituted and organized, we used a micro-Computed Tomography (micro-CT) technique, so far predominantly used for medical diagnostics (Latief et al., 2017) or for inspecting industrial components (Makeev et al., 2010), and recently used to explore the living world (Rawson et al., 2020). The micro-CT technique is a non-destructive method able to provide the 3D morphological and contextual details of collected specimens taking a series of x-ray radiographs of a subject and reconstructing it, including its intrinsic composition.

In this paper, we focus on showing the contribution of 3D-representations at different scales to study marine ecosystems. 3D-reconstructions are presented as 2D-views and internet links to videos are provided, enabling users to navigate in the 3D environments. Our study area is located in the Lacaze-Duthiers Canyon in the Gulf of Lion (western Mediterranean Sea) where hard substrates and vertical walls are covered by extensive cold-water coral assemblages built up by structure-forming scleractinians. We focus on: (1) 3D-bathymetric maps (5-m and 1-m resolution) to analyze the geological complexity of the substrate where coral colonies settle; (2) 16 photogrammetric models of cold-water coral assemblages (2 cm accuracy), showing how species are organized in the ecosystem; and (3) micro-CT scans (20–100 μm resolution) of five deep-sea scleractinian species to understand their intrinsic organisation (*Madrepora oculata*, *Desmophyllm pertusum*, *Desmophyllum dianthus*, *Caryophyllia smithii*, *Dendrophyllia cornigera*).

2. Materials and methods

2.1. 3D-Reconstructions produced with acoustic data for the geological setting scale (Bathymetry)

Acoustic data was collected during the CALADU expedition in October 2019 (R/V L'Europe; Ifremer https://doi.org/10.17600/18000929). We used a hull-mounted MBES Kongsberg ME70 (90 kHz) to collect bathymetric data of the canyon's flanks at a grid cell size of 5 m. We also used a Kongsberg EM2040 (300 kHz) mounted on the hybrid ROV (H-ROV) Ariane operated by Ifremer to build higher resolution maps at a grid cell size of 1 m. We initially used the MBES installed on the H-ROV in a downward-looking position, but afterwards it was changed to a configuration with a 45° angle position (Fig. 1), to collect data on vertical cliffs, while navigating ~50 m away from the seafloor.

We collected bathymetric data with Ariane's MBES during three dives (Fig. 2): Dive 139–01 with MBES in a downward-looking position and Ariane navigating along the western flank; Dive 140–02 with MBES installed in a 45° position and Ariane navigating up-slope across the western canyon flank (this was a very short survey because Ariane was trapped in a longline and had to cut the optical fiber which ended the dive); Dive 141–03 with MBES installed in a 45° position and Ariane navigating up-slope in the head region and mapping several walls and overhanging reliefs.

Post-processing of MBES data was carried out with the software GLOBE, ©Ifremer (GLobal Oceanographic Bathymetry Explorer) that offers processing and display solutions of multi-sensor data within a single 3D environment represented as a globe. The software is mainly used at present for processing, analyzing and displaying acoustic data (Poncelet et al., 2020).

2.2. 3D-Reconstructions produced with photographic images for the coral assemblage scale (Photogrammetry)

The images collected with the H-ROV Ariane were recorded using a tilt-mounted photo camera (Nikon D5200). Images were used to build 3-Dimensional (3D) models of coral assemblages living in the Lacaze-

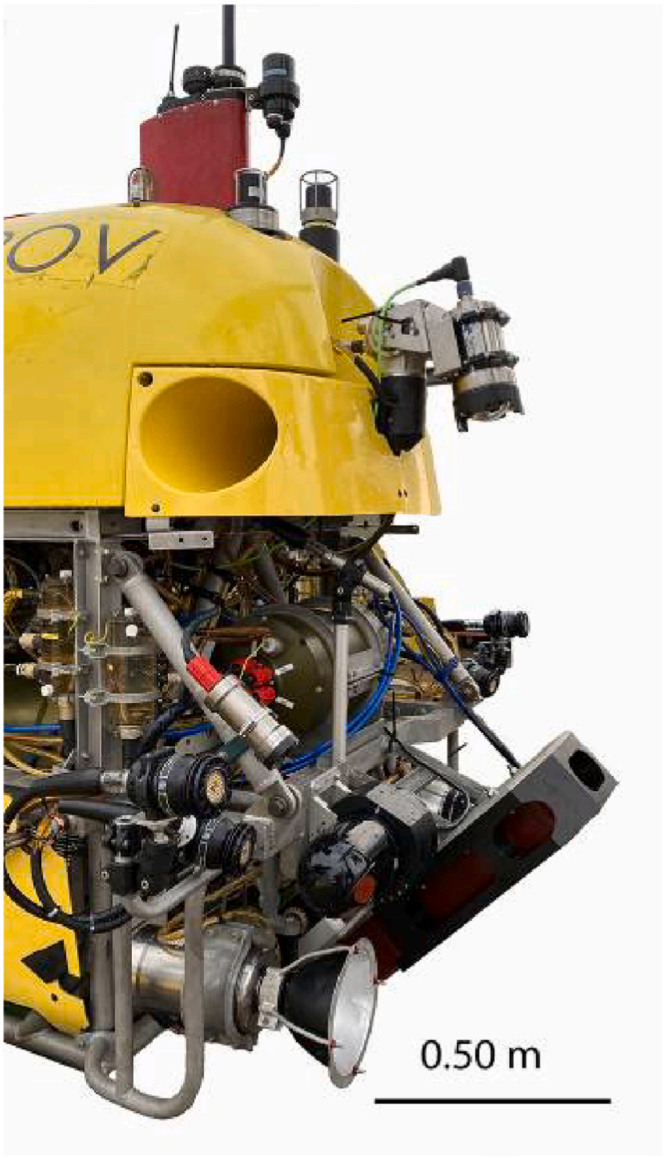

Fig. 1. Image of Ariane H-ROV with the Kongsberg EM2040 Multibeam Echosounder installed with a 45° angle.

Duthiers Canyon. During each dive, 1 h was dedicated to photo and/or video acquisition intended for later mosaic building. This acquisition required a specific navigation procedure in order to obtain several images of the same scene from several viewpoints; also, these images must overlap by at least 50% (Arnaubec et al., 2015). 3D-models were built using the 'Structure from motion' technique available in the Matisse software available on a github (Arnaubec et al., in prep.). The number of images used to build 3D-models were 1913, 1065, 1560 and 2676 for dives 142–04, 143–05, 144–06 and 145–07, respectively.

The Ifremer 3D Metrics software was used to visualize photogrammetric models and geolocalize, count and measure two different species of coral colonies: *D. pertusum* and *M. oculata*. Coral densities (colony number per m^2) were calculated by dividing the number of colonies plotted on each 3D model and the measurement of the reconstructed 3D surfaces at each location. Lost fishing gears were also mapped, lines were drawn on the models to measure their lengths, and their density (line number per m^2) was calculated at each location. Statistical analyses were then performed using XLSTAT for Excel (Addinsoft, 2019). Non-parametric Mann-Whitney tests, validated with 1000 Monte Carlo simulations, were applied to compare depth distributions of both species

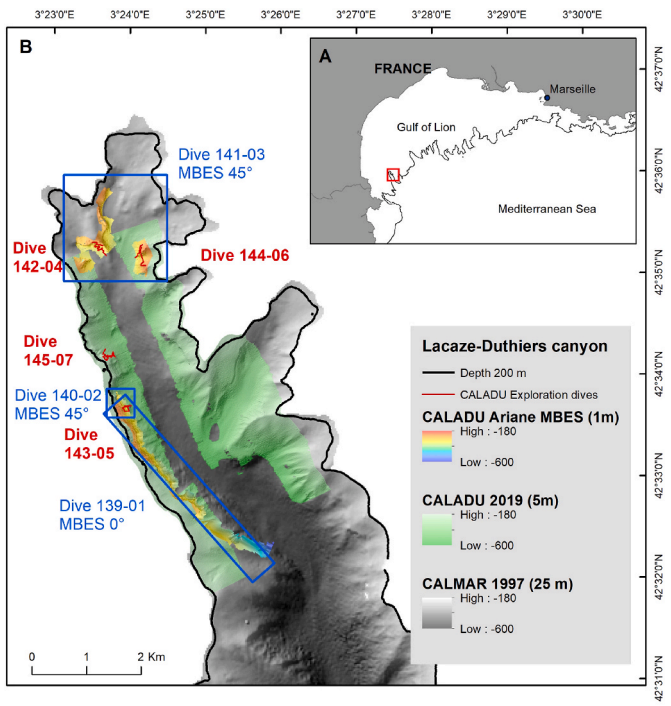

Fig. 2. Lacaze-Duthiers Canyon head. A: Location in the Gulf of Lion, Western Mediterranean Sea. B: Previous hull-mounted multibeam bathymetric data with 25-m pixel size are shown in grey scale, new hull-mounted multibeam bathymetric data with 5-m pixel size are shown in green scale, H-ROV multibeam data with 1-m pixel size are shown on a color scale and the tracks of exploration dives with optical images are represented as red lines.

at each site.

Height measurements, from the bottom to the top of each colony, were used for sizes (cm) as described in Fabri et al. (2019). When corals were nested, making inaccessible the base of the colony for measurements, the total heights of colonies were thus slightly underestimated. We assumed precision of measurements to be of 1 cm (Istenič et al., 2019). A non-parametric Kruskal-Wallis test was used to compare mean heights of *D.pertusum* and of *M. oculata* at the four locations. The non-parametric Kolmogorov-Smirnov test was used to compare the height distributions on sites (two-by-two), for each species. Gaussian mixture models were run to identify the different size groups at each location for the same species.

3D representations make it possible to visualize a scene of several square meters, so many colonies could be observed at a single glance in the same place. We noted that the colonies were all facing the same direction at the same location. Following the hypothesis that coral colonies face prevailing currents (Freiwald et al., 2009; Vertino et al., 2010), we were able to deduce those from the general orientation of the colonies on each 3D model. As the 3D models are georeferenced in space, we entered this orientation in a GIS and deduced the dominant currents on each location for which we had a photogrammetric model.

2.3. 3D-Reconstructions produced with radiographic data for the individual scale (Micro-computed tomography)

Coral samples were collected with Ariane H-ROV in the Lacaze-Duthiers Canyon and were immediately frozen on board (−40 °C). The samples were examined after defreezing without any particular drying treatment. The soft tissues may have evolved slightly during the scan, but since they occupied a small relative volume, the reconstruction of the skeleton was only slightly affected. Micro-CT analysis allowed investigating the morphology of our samples skeletons in a non-destructive manner. Micro-CT imaging involves the recording of two-

dimensional x-ray images (over 1000) from various angles (trough 360°) around a sample, with a circular (1440 projections) or helicoidal (up to 8640 projections) trajectory. The digital radiographs reveal the attenuation capability of the sample. The 3D dataset is then reconstructed and the resultant 3D-rendered volume allows for the multidirectional examination of a sample. Micro-CT imaging produces a 3D distribution of linear attenuation coefficients that are related to mass density. However, because we did not add a calibration phantom, the images are not calibrated and density values cannot be compared accross samples. Coral skeleton densities can be highlighted with different colors. We have chosen to represent the density gradient in color, from high densities in pink, to blue and yellow for low densities. When necessary, some density classes were represented in a transparent color in order to enable an interior view of the skeleton.

The micro-CT instrument we used (Easy Tom XL/RX Solutions) uses a tungsten x-ray source with 20–150 kV energy and 0–500 μA intensity. It is equiped with a 1516x1920 pixels CCD camera and builds 3D images with a minimal voxel size of 4 μm. Specimens were scanned with 100 kV and 300 μA source settings, and a 1 mm aluminium high-pass filter. The x-ray source and detector were fixed around a rotating sample, giving access to resolutions in the micrometer range (4–150 μm; higher image resolution for smaller samples; higher voltage for dense or thick material) (du Plessis et al., 2017). The micro-CT scanning was performed at the SUBATECH Laboratory (UMR6457 – IMT Atlantique – CNRS - University of Nantes, France). 3D representations of the scleractinians were post-processed and visualized with the MeVisLab software. Dynamic views of the micro-CT scans were produced using the Dragonfly 2020.2, Object Research System (ORS) Inc, Montreal, Canada, 2020 (www.theobjectscom/dragonfly).

3. Results

3.1. 3D-Reconstructions produced with bathymetric data for the geological setting scale (Bathymetry)

The bathymetry acquired with the hull-mounted MBES provided higher resolution morphological information at a 5 m grid, compared to the previous bathymetry from the same area collected back in 1997, at a 25-m grid resolution (Fig. 2). The seafloor representation allowed better definition of the canyon's flanks and morphological features, where rough and steep areas with sharp edges and rocky outcrops were clearly evidenced. Those areas were selected and dedicated to collecting higher resolution maps using the MBES mounted on the H-ROV.

This high-resolution bathymetry (1 m) allowed observing lithified sedimentary strata along the flanks of the canyon, with alternations of steep and hard rocky terrains with flat areas covered by fine sediment (Fig. 3). Such layering reflects the stratification of the sedimentary deposits in which the canyon incises, and seems to have been carved out by currents, causing harder materials to protrude and form small overhanging ledges. This is particularly noticeable at the head of the canyon. When overhangs of lithified sediment strata are no longer stable, they break down and collapse creating a boulder field, clearly visible at the foot of the north cliff (Fig. 3, dive 142–04). A fly-through video showing sharp bathymetric structures in the canyon is available on https://image.ifremer.fr/data/00746/85829/(Fabri et al., 2022c).

All these geological morphologies were checked with optical imagery during exploration dives. We could see that both hard substrates, lithified sediment and boulders, were often used as places of fixation for benthic organisms such as scleractinians (*M. oculata* and *D. pertusum, but also D. dianthus, C. smithii* and *D. cornigera)*, oysters (*Neopycnodonte cochlear*) or many sponges and serpulids.

3.2. 3D-Reconstructions produced with photographic images for the coral assemblage scale (Photogrammetry)

Coral assemblages were reconstructed at several locations in the canyon. Both colonial species, *M. oculata* and *D. pertusum,* were plotted on photogrammetric models, so they could be geolocalized in space, with coordinates and depth. Dots plotted on photogrammetric models were then reported on bathymetric models (Fig. 3). A traveling video giving a 3D-representation of cold-water coral assemblage is available in open access on https://image.ifremer.fr/data/00746/85828/(Fabri et al., 2022a).

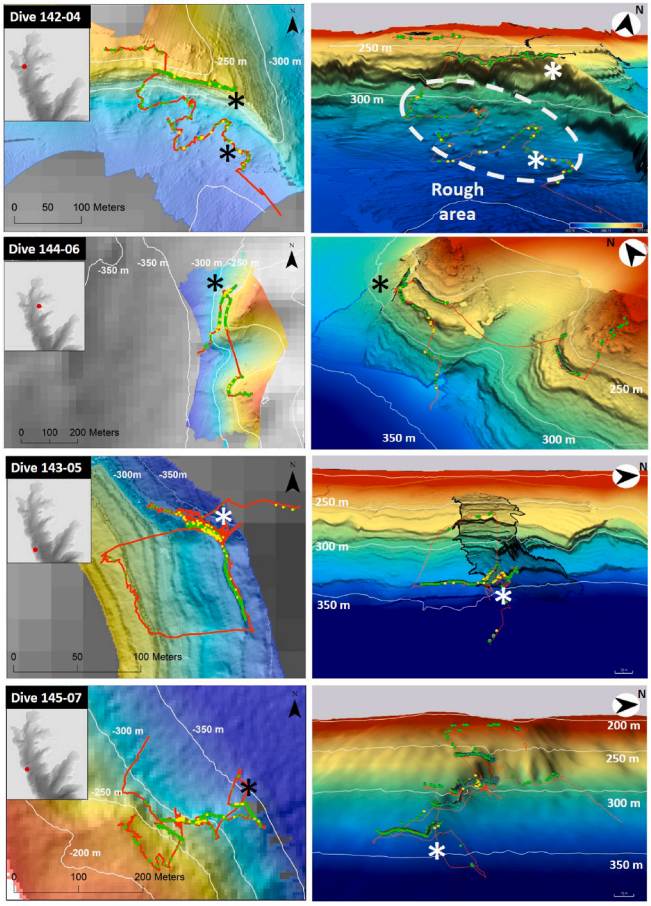

Fig. 3. 3D-Representation of the canyon's flanks, with high resolution bathymetry (1-m pixel size on sites of dives 142–04, 143–05, 144–06 and 5-m pixel size on the site of dive 145–07). Navigation tracks are represented as red lines. Coral colonies have been reported from photogrammetric models. Colonies *of M. oculata* and *D. pertusum* are reported as green and yellow dots, respectively. Asterisks (black or white) indicate locations of 3D representations shown in Fig. 7.

3.2.1. Spatial and vertical distribution of both coral species

The northernmost reconstructed area was on a wall of the northern spur of a western tributary of the canyon head (Dive 142–04; depth range 237–340 m; Figs. 2 and 3). We started to explore the foot of the wall to check the rough area visible on the bathymetry and saw they were hard blocks on which few colonies of *D. pertusum* had settled, at a depth of 340 m. Then, we explored the wall and as soon as we encountered coral colonies, we navigated to follow coral coverage. This obliged us to proceed horizontally between 260- and 280-m depth. We initially moved East along the stratum, following the coral colonies, then returned along the same track (Fig. 3).

We also explored the two spurs of the eastern canyon head tributary (Dive 144–06; depth range 203–335 m) Figs. 2 and 3). We started at the bottom of the northern spur, 335 m depth, and went up the slope until we found several corals, then we followed the coral colonies. They were aligned along strata at 255-m and 272-m depth. However, they were not present along the entire length, and their occurrence depended on the

orientation of the stratum and were mostly found on substrates oriented northward (*i.e.* up-canyon). When we finished exploring the stratum at 272-m depth on the northern spur, the ROV traveled through the water to reach the stratum at the same depth on the southern spur where we also found and observed coral colonies. We finished this dive by exploring the top of the spur where we saw some blocks with coral colonies.

The other two explorations took place on the western flank of the canyon (Dives 143–05 and 145–07; depths ranges 334–384 m and 189–313 m respectively; Figs. 2 and 3). The targeted areas were steeply sloping regions (>50°), suggesting the presence of cliff failure scars. Indeed, we found the most abundant colonies on these two target sites. We started explorations at the bottom of the cliff, 384 m and 313 m depth, then followed the coral colonies as soon as we found them. Areas with big colonies of high density were in highly complex environments. The more complex the topography, the taller the colonies were, the more entangled lost fishing longlines were present. At a very complex location explored during dive 145–07 we found orange colonies of *D. pertusum*, next to white ones (Fig. 4). At the periphery of these high-density areas, where substrates were no longer visible, colonies were still aligned along the geological strata inferred on the bathymetric map. At the location of dive 145–07, the 3D-reconstructions clearly shows that colonies were spread over consecutive strata heads at 330, 308, 292, 386, 273, 255 and 220 m depth, especially on outgrowths facing north (Fig. 3). In this rugged environment, lost fishing longlines were numerous and made navigation dangerous. Sometimes it was even difficult to get close to the cliff because the consecutive longlines increased the risk of entangling the H-ROV.

Bathymetrical distributions observed during the CALADU cruise ranged from 339 to 254 m deep for *D. pertusum* and from 339 to 214 m deep for *M. oculata*. At three sites (dive 142–04, dive 144–06 and dive 145–07), colonies of *D. pertusum* were observed deeper than those of *M. oculata* (Mann-Whitney unilateral test, p-value < 0.01) (Fig. 5). For dive 143–05, a significant difference between depths of both species was also found (Mann-Whitney unilateral test, p-value < 0.01), *D. pertusum* were conversely located at shallower depths (332 m) than those of *M. oculata* (333 m), and were found in higher proportion than at other sites (31% of the coral colonies) (Table 1). This location is also the most southerly one, the furthest from the head of the canyon. Conversely, the shallowest locations (Dives 144–06 and 142–04; 262 m) are where we found the highest proportion (97 and 96%) of *M. oculata*. Those locations are at the head of the canyon and on the eastern flank.

3.2.2. Surface coverage and colony densities of both coral species

A total area of 4370 m^2 at the head of the Lacaze-Duthiers Canyon was reconstructed, corresponding to 1041, 568, 1290 and 1471 m^2 at dives 142–04, 143–05, 144–06 and 145–07, respectively (Table 1).

The coral populations had a mean density of up to 4.3 colonies per m^2 including both species together. Populations of *M.oculata* and *D. pertusum* had maximums of 4 and 2.8 colonies per m^2, respectively for dive 145–07, but on different strata heads (Table 1). This density calculation was performed using the complete reconstructed area, which was correct for *M oculata* as they are widely distributed; however *D. pertusum* colonies had a more concentrated distribution. In some areas, *D. pertusum* density reached 4 colonies per m^2 over areas of about 100 m^2; these high density areas were northwards oriented locations on dives 143–05 and 145–07 (Table 1). For *M. oculata* we measured several areas ranging between 100 and 600 m^2 with densities exceeding 3 colonies per m^2 (Table 1). We intentionally targeted high density coral areas so these densities are not indicative of general canyon habitat coverage.

We can also noticed that the global density of *D. pertusum* was higher (0.6 and 0.5 col./m^2) at both sites located on the western flank (dives 143–05 and 145–07) compared to the two others (0 and 0.1 col./m^2) located in the head of the canyon (Table 1).

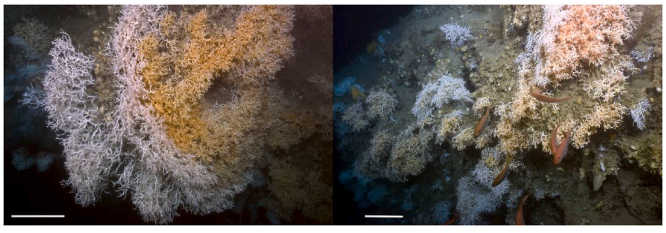

Fig. 4. Orange colonies of *D. pertusum* seen on the western flank of Lacaze-Duthiers Canyon (dive 145–07, depth 280 m). Scale bar is 25 cm.

3.2.3. Size structure of coral populations

A total of 5387 colonies were measured, 851 colonies of *D. pertusum* and 4536 colonies of *M. oculata*. *Desmophyllum pertusum* had an average height of 28 cm (standard deviation sd = 15 cm) while that of *M. oculata* was 18 cm (sd = 7 cm) (Fig. 6).

The maximum height of *D. pertusum* was 88 cm, and the maximum height of *M. oculata* was 50 cm, they were seen during dives 143–05 and 145–07 at around 330 m depth. There were several bushes of similar big colonies close together; the size of the bushes reached 2.5 m in length for *D. pertusum* and 1.8 m for *M. oculata* (Fig. 7).

Both species showed differences in average height between sites (non-parametric Kruskal-Wallis test; p-value <0.05) (Fig. 6).

With regard to *D. pertusum* populations, the size-frequency diagram shows a different pattern in size distribution at each dive location (Fig. 6). At the location of dives 142–04 and 144–06, only 47 and 76 colonies respectively could be seen and measured, and they were only small ones (average size of 16 cm). On the western flank for dives 143–05 and 145–07, we performed 362 and 370 measurements of *D. pertusum*, showing 3 and 2 statistical groups, respectively, according to Gaussian mixture models (Fig. 6). For dive 143–05, 33% of the population was in the small size group (mean size 16 cm), while the rest of the population was in groups of mean sizes of 28 cm (42%) and 52 cm (25%). For dive 145–07, there were only two groups of colonies, with mean sizes of 26 cm (71%) and 44 cm (29%).

With regard to *M. oculata* populations, the size-frequency diagram shows a similar pattern in size distribution for each dive location (Fig. 6). When looking at all the sites together, the population structure is composed of 3 statistical groups according to Gaussian mixture models, the largest group (53% of the population) is composed of colonies with a mean size of 18 cm (Fig. 6). The rest of the population is distributed in groups with mean sizes 12 cm (26%) and 27 cm (21%). This distribution is similar to that of dive 145–07. At the three other sites, *M.oculata* populations showed similar distributions (Kolmogorov-Smirnov, p-value > 0.01). Colonies were distributed in two groups of mean sizes 15 cm (70%) and 23 cm (30%).

3.2.4. Coral colony orientations

Following the hypothesis that coral colonies face prevailing current (Freiwald et al., 2009; Vertino et al., 2010), we can deduce current flows from the photogrammetric models (Fig. 7).

On the eastern flank, at dive location 144–06 (Figs. 2 and 3), all the coral colonies were clearly oriented in the same direction, all facing north (*i.e.* towards the main canyon head) at the canyon's axis. However, they were facing east in gullies as the prevailing current at those locations likely came from the tributaries at the eastern canyon head (Fig. 7).

Similarly, on the western flank, for dive locations 143–05 and 145–07 (Figs. 2 and 3), all the coral colonies were clearly oriented in the same direction, all facing north (i.e. towards the main canyon head) in the canyon's axis, but facing west in gullies as the prevailing current likely came from the tributaries at the western canyon head (Fig. 7).

For dive location 142–04 (Figs. 2 and 3) on the northern wall, coral colonies did not show a preferential orientation though mainly faced downwards (Fig. 7).

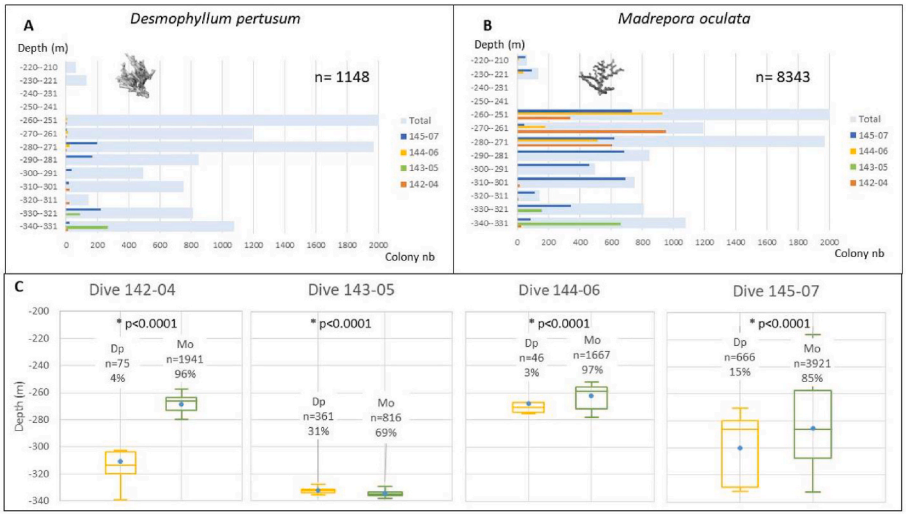

Fig. 5. Bathymetrical distribution for both species for each dive. A and B: Histograms of depth distribution for each of both species, for each dive; C: Box plot of depths distribution, *D. pertusum* (Dp) on the left, *M. oculata* (Mo) on the right for each dive. Mann-Whitney tests were performed to confirm the differences in depth distribution between both species at each site. Blue dots represent average depths, horizontal bars in boxes represent medians. "n" is the number of colonies for a species; "%" is the percentage of species colonies out of the total number counted on the 3D representations for each dive.

Table 1
Mean depths and surface coverage of the 16 3D-models, colony numbers for both species (D. pertusum and M. oculata), as well as lengths of longlines (m) measured on each surface reconstructed in 3D (m^2) and their densities. Percentage (%) gives the number of colonies of one species out of the total number of colonies on 3D representations. * Locations where D. pertusum density was 4 colonies per m^2 when considering only the area where the species is present (100 m^2) and not the whole mosaic.

SITE	Surface (m^2)	Mean depth (m)	*D. pertusum*			*M. oculata*			Both species		Longlines	
			Number	Density (col./m^2)	Percentage %	Number	Density (col./m^2)	Percentage %	Number	Density (col./m^2)	length (m)	Densities (m/m^2)
142–04	**1041**	**−270**	**75**	**0.1**	**4**	**1941**	**1.9**	**96**	**2016**	**1.9**	**132**	0.13
Bottom	*422*	*−320*	*66*	*0.2*		*47*	*0.1*		*113*	*0.3*	*16*	*0.04*
Wall	*619*	*−267*	*9*	*0.0*		*1894*	*3.1*		*1903*	*3.1*	*116*	*0.19*
143–05	**568**	**−333**	**361**	**0.6**	**31**	**816**	**1.4**	**69**	**1177**	**2.1**	**110**	0.19
Stratum 333 m	*315*	*−335*	*9*	*0.0*		*422*	*1.3*		*431*	*1.4*	*82*	*0.26*
***Strata 333 m (North face)**	*253*	*−332*	*352*	*1.4*		*394*	*1.6*		*746*	*2.9*	*28*	*0.11*
144–06	**1290**	**−262**	**46**	**0.0**	**3**	**1667**	**1.3**	**97**	**1713**	**1.3**	**249**	0.19
Stratum 255 m	*360*	*−256*	*10*	*0.0*		*930*	*2.6*		*940*	*2.6*	*108*	*0.30*
Stratum 272 m	*436*	*−272*		*0.0*		*221*	*0.5*		*221*	*0.5*	*71*	*0.16*
***272 m (North Face)**	*310*	*−272*	*36*	*0.1*		*470*	*1.5*		*506*	*1.6*	*53*	*0.17*
South summit	*184*	*−224*		*0.0*		*46*	*0.3*		*46*	*0.3*	*17*	*0.09*
145–07	**1471**	**−288**	**666**	**0.5**	**15**	**3921**	**2.7**	**85**	**4587**	**3.1**	**230**	0.16
Stratum 223 m	*247*	*−221*		*0.0*		*149*	*0.6*		*149*	*0.6*	*16*	*0.06*
Stratum 255 m	*235*	*−256*		*0.0*		*733*	*3.1*		*733*	*3.1*	*57*	*0.24*
Stratum 272 m	*171*	*−272*	*6*	*0.0*		*612*	*3.6*		*618*	*3.6*	*43*	*0.25*
***Central part 286 m (North Face)**	*366*	*−287*	*399*	*1.1*		*1181*	*3.2*		*1580*	*4.3*	*75*	*0.20*
Stratum 292 m	*54*	*−293*		*0.0*		*13*	*0.2*		*13*	*0.2*	*15*	*0.27*
Stratum 308 m	*202*	*−307*	*17*	*0.1*		*806*	*4.0*		*823*	*4.1*	*14*	*0.07*
***Stratum 330 m (North Face)**	*88*	*−329*	*244*	*2.8*		*52*	*0.6*		*296*	*3.4*	*0*	*0.00*
Stratum 330 m East side	*108*	*−330*		*0.0*		*375*	*3.5*		*375*	*3.5*	*11*	*0.10*
TOTAL	**4370**		**1148**	**0.3**	**12**	**8345**	**1.9**	**88**	**9493**	**2.2**	**721**	**0.16**

3.2.5. *Lost fishing gears*

A total length of 721 m of longlines was measured on a surface area of 4370 m^2, which mean 0.16 m of longlines were observed on each square meter reconstructed (Table 1). Among the four surveyed sites, the highest longlines densities were observed at dive locations 143–05 and 144–06 on both flanks (0.19 m/m^2), with a maximum (0.30 m/m^2) observed at dive location 144–06 at 255 m depth (Table 1).

It should be noted that only old longlines, covered by epifauna (oysters, coral colonies, tube worms) could be reconstructed and measured. Recent longlines, not yet covered by epifauna, were too thin to be seen on the photogrammetric models. In addition, as lost longlines floating in the water were hazards for Ariane, because it could get snagged in the structure and tangled in the optic fiber, they were avoided when seen. Thus, they do not appear on the photogrammetric models (Fig. 8). For these reasons, the census of longlines was underevaluated.

In addition to longlines, four fishing nets were observed and reconstructed on photogrammetric models (Fig. 8). At dive location 142–04 a

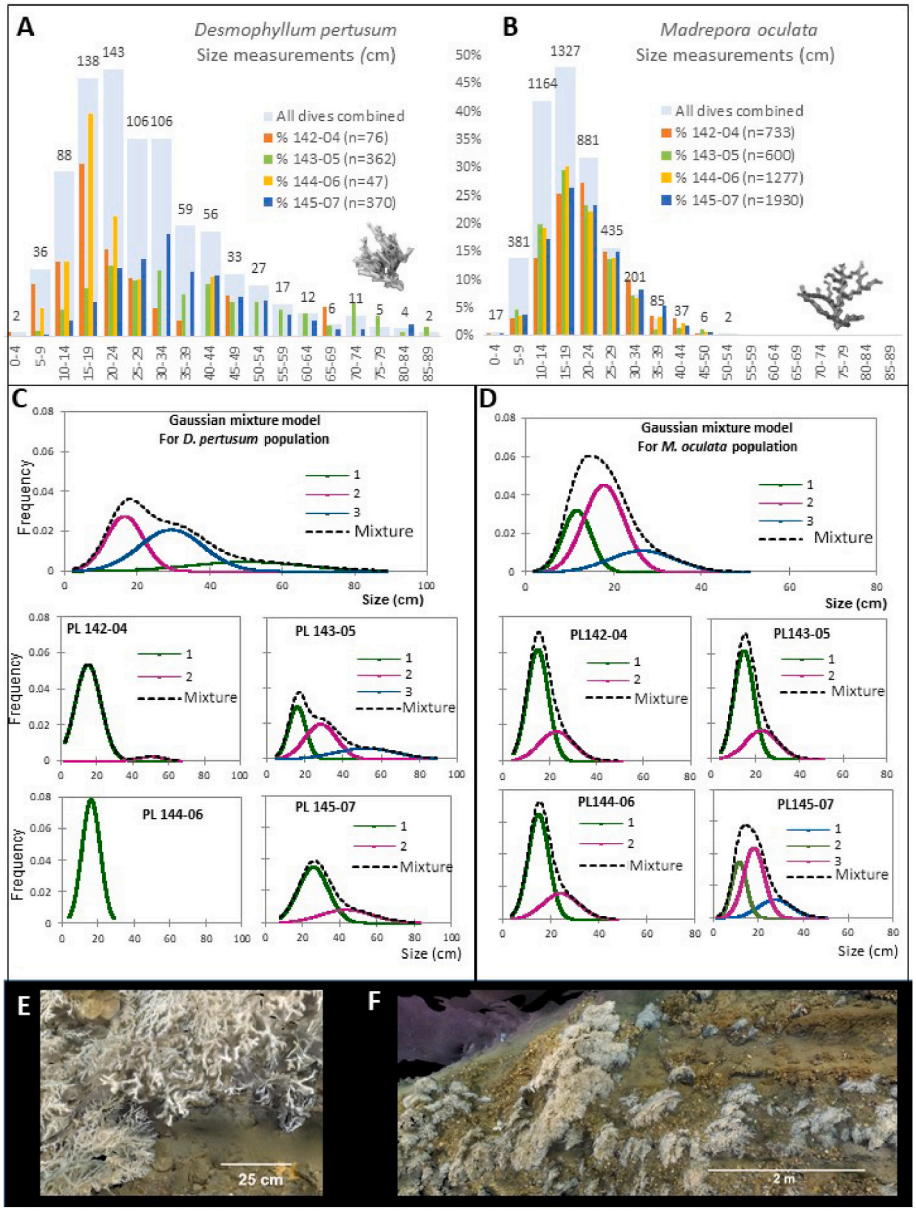

Fig. 6. Height distribution of both species measured from photogrammetric models. Size frequency and Gaussian mixture models of the whole population and the population at each dive location for *D. pertusum* (A and C) and *M. oculata* (B and D). E: Zoom on a model showing colonies of both species of more than 25 cm; F: Zoom in a model showing a bush of *M. oculata* approximately 2 m long.

piece of net was seen on a large rock (1 m^2), at dive location 143–05 two large nets were seen (46 and 50 m^2 at 334 and 280m depth, respectively) and at dive location 145–07 one very large net was measured (130 m^2 at 223 m depth). No nets were observed at dive location 144–06. Nets were usually seen covered by oysters.

3.3. 3D-Reconstructions produced with radiographic data for the individual scale (Micro-computed tomography)

This dataset was created with the purpose of visualizing the morphological criteria of coral skeletons in three dimensions. The specimens looked at are scleractinians, also called stony corals because of their external skeleton made of aragonite. Scleractinians belong to the subclass of Hexacorallia because of their hexameral symmetry. The skeleton is composed of solitary or colonial calices depending on the species. Calices are composed of internal vertical partitions (radiating lamellae named septa), and optional ornamentations (a columella is the junction of septa at the bottom of the calice, a pali is an ornamentation on a septum) arising from the basal plate and arranged in multiple cycles of several alternating orders (Zibrowius, 1980; Altuna and Poliseno, 2019). Videos of the inside of the skeleton of the five scleractinian species sampled during the CALADU cruise are available on https://image.ifremer.fr/data/00745/85674/ (Fabri et al., 2022b).

*Madrepora oculata (*family *Oculinidae)* is a colonial species with a zig-zag shaped skeleton forming large-size colonies. The calices examined are around 6 mm high and 3 mm in diameter, voxel size 9 µm. Micro-CT scans show the skeleton composed of carbonates of different densities (Fig. 9A). High density material (pink) composes the external part of the main skeleton of the colony. Intermediate density material (blue) is located inside the skeleton between the basal part of a calyx and the calyx underneath. Low density material (yellow) composes the internal ornamentations (speta and columella). Longitudinal cuts show that calices are separated from each other. Transversal cuts show that calices harbor 24 septa organized in 3 alternating cycles. First order septa are

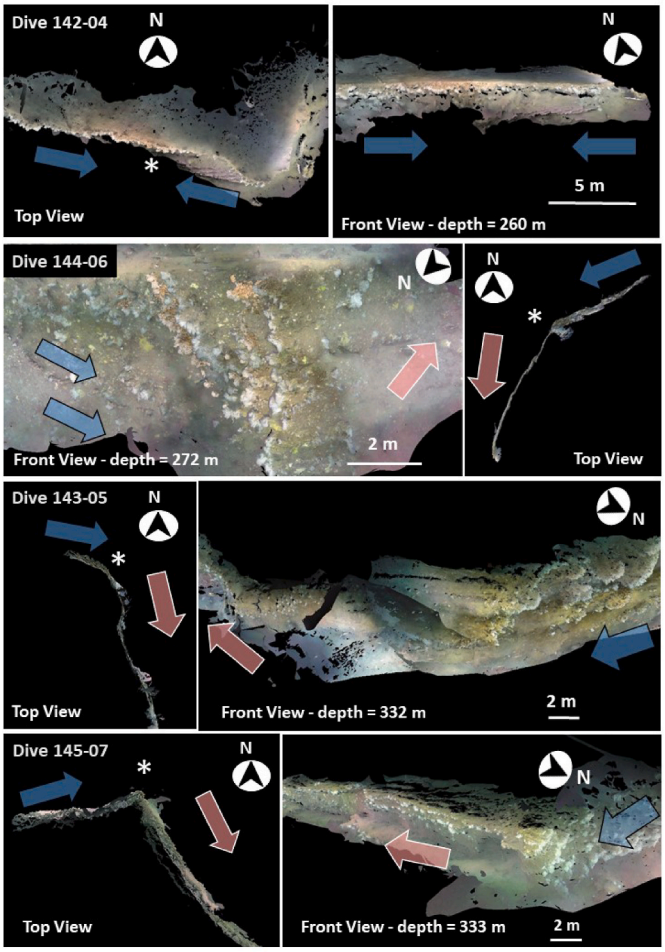

Fig. 7. Top and front views showing 3D-representations of coral assemblages. The white asterisk on the top views shows where the front viewpoint is located. Arrows show current flows deduced from the orientation of colonies, the blue and black arrows show currents coming from the canyon flank tributaries, pink and white arrows show currents in the main canyon axis (as on Fig. 10). The locations of these representations are indicated by asterisks on Fig. 3.

very close together at the bottom of the calice and are joined so that they form a columella. The branched surface shows narrow, slightly concave furrows. The position of a polyp underneath the polyp of the previous generation attests that budding occurs by external extension of the side of a calyx (extracalicinal).

Desmophyllym pertusum (syn. *Lophelia pertusa*, family *Caryophyliidae*) is a colonial species with a skeleton that occupies space multidirectionally (Fig. 9B). The calices examined are those from a distal branch and measured around 9 mm high and 4 mm in diameter, voxel size 10 μm. High density material (pink) composes the external part of the main skeleton of the colony. Intermediate density material (blue) composes internal parts of the skeleton and calices, and is covered by a lower density material (yellow) arranged to form the internal organization. Low density material (yellow) covers both the inside and the outside of the main skeleton. Micro-CT scans clearly show that calices communicate with each other by a thin canal connecting buds of successive generations. Calices harbor 24 septa organized in 3 cycles. First order septa are very close together at the bottom of the calyx and are joined by thin horizontal structures in the basal parts of each calyx (Fig. 9B, green arrow). No columella is present. First order septa are larger and ornamented with granularities. The branch surface is smooth. The position of recent buds on top of previous generation buds attest that budding occurs by lateral extension of the calice border (intracalicinal).

Desmophyllum dianthus (family *Caryophyliidae*) is a fixed solitary coral. Our specimen was collected broken in its basal part and is 5 cm high and 3.2 × 2.7 cm in diameter, voxel size 25 μm (Fig. 9C). The skeleton is composed of carbonates of different densities, high density outside the calyx (pink) and intermediate density inside (blue), especially at the top of the calyx where septa expand. In this top part the septa are composed of even less dense material (yellow). Carbonate density is not regularly distributed. The basal part shows thin internal horizontal structures (Fig. 9C, green arrow). The septa are arranged in 5 cycles, creating a total of 96 septa on our specimen. Large specimens can show 6 cycles of septa leading to 192 septa (Zibrowius, 1980).

Caryophyllia smithii (family *Caryophyliidae*) is a solitary coral that was sampled on hard bottoms and measures 1.7 cm high and 2 × 1.5 cm in diameter, voxel size 16 μm. Micro-CT scans show granulations on the external part of the skeleton and on first order septa, and the skeleton is composed of carbonates of different densities (Fig. 9D). The external part of the skeleton is composed of granular hard material (pink) oriented longitudinally in prominent ribs (costae). Septa and columella are of lower density material (blue). On transversal cuts we can observe 4 circles of septa with palli. Septa of the first order S1 and second order S2 are sub-equal, while S3 and S4 are shorter. Hexaradial symmetry is not obvious as there are 8 S1 and 8 S2, but fewer S3 and S4. A fascicular columella composed of twisted lamellae is clearly present with very dense material in its basal part (pink) and intermediate density material in its upper part (blue).

Dendrophyllia cornigera (family Dendrophylliidae) is a colonial species composed of successive generations of budding (Fig. 9E). Calices of our specimen are around 4 cm high and 2 cm in diameter, voxel size is 58 μm. The skeleton is composed of material of different densities arranged along a longitudinal axis, as can be seen on the micro-CT images. The external part of the skeleton is composed of hard density material (pink) arranged in streaks with longitudinal ribs. Transversal cuts show septas arranged in multiple cycles following a "Pourtales plan" with septa forming triangles, and a central columella. The septa and main skeleton are porous.

4. Discussion

In this paper, multiple imaging methods of varying scales and resolutions were employed to illustrate the contribution of 3D-visualization techniques for studying marine benthic ecosystems.

4.1. 3D-Reconstructions produced with acoustic data for the geological setting scale (Bathymetry)

Recent studies in the Lacaze-Duthiers Canyon dealing with cold-water corals have mainly focused on their microbiome (Chapron et al., 2020a, 2020b, 2021) and their growth with regard to anthropogenic impacts like plastic exposure and climate change (Lartaud et al., 2017a, 2017b; Galand et al., 2018, 2020; Mouchi et al., 2019). Habitat mapping and exploration were not completed after the Medseacan cruise in 2009 (Fiala-Medioni et al., 2012; Watremez, 2012; Gori et al., 2013; Fabri et al., 2014), therefore, no recent bathymetric data has been collected in the Lacaze-Duthiers Canyon since the CALMAR cruise in 1997 (Berné et al., 1999). Our investigation provides up to date data in the head of the canyon, collected with the use of a MBES installed with an angle of 45° in front of the H-ROV Ariane able to provide information on the complex topography in which cold-water corals settle and live, such as the flanks and walls of canyons (Lastras et al., 2016; Robert et al., 2017; Lo Iacono et al., 2018; Price et al., 2019).

The geological features were mapped in 3-dimensions which revealed very sharply defined features with vertical walls created by sub-parallel lithified sedimentary strata (Fig. 3). These stratigraphic deposits correspond to sedimentary sequences built on the Gulf of Lion margin during glacioeustatic (interglacial/glacial) cycles over the last 540,000 years (Rabineau et al., 2005). The network of submarine canyon incisions in the Gulf of Lion corresponds to the imprint of

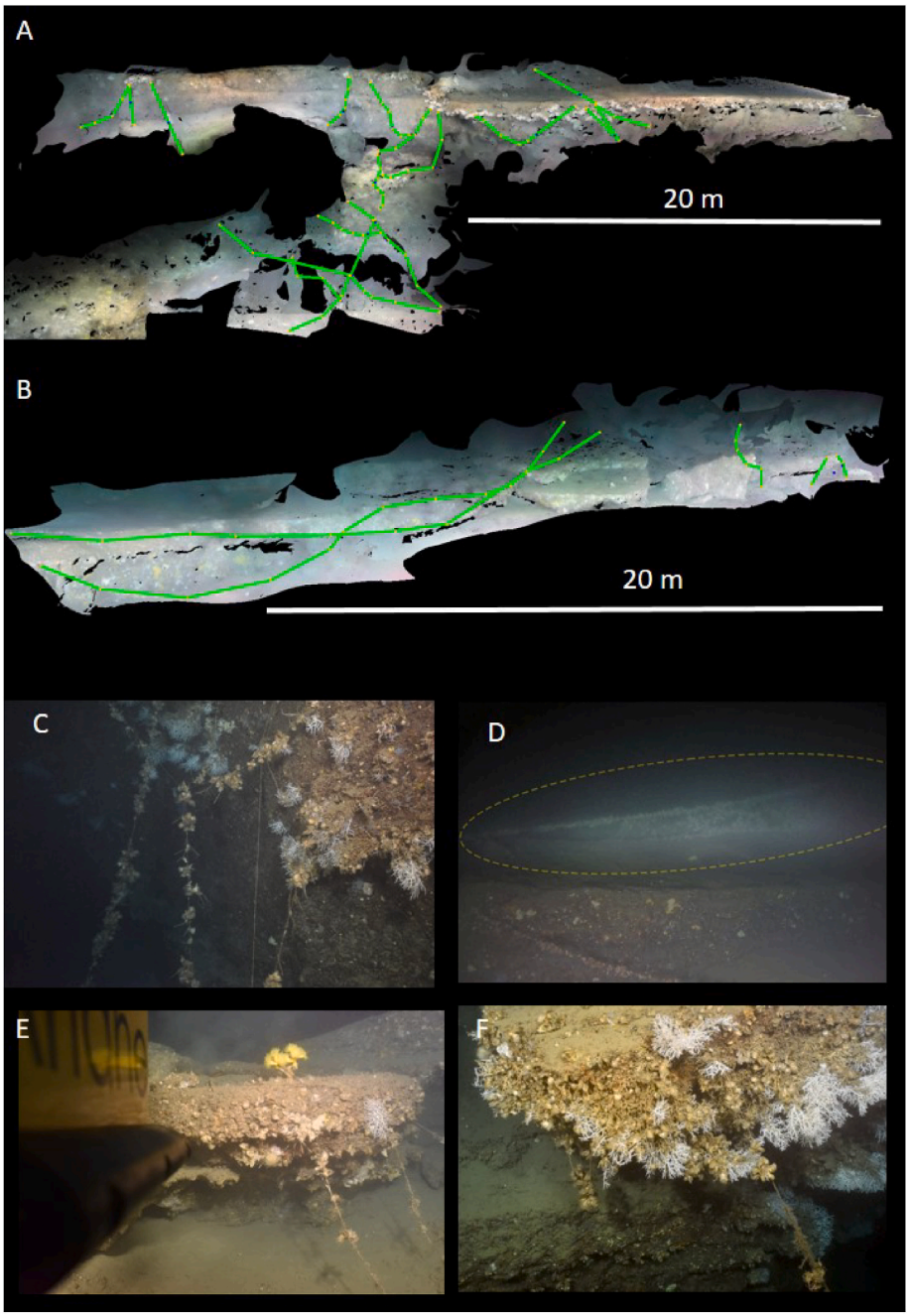

Fig. 8. Lost fishing gears. A and B: 3D-Representations of a longline (dive 142–04) and a net (dive 143–05) highlighted as green lines; C. Longlines dive 143–05; D. Image of the net reconstructed above on which we can see oysters hanging, dive 143–05; E and F. Longlines, dive 145–07.

turbidity currents that eroded these sedimentary deposits during phases of connection to rivers (hyperpycnal turbidity current), most likely during low sea levels, when a high detrital sediment supply (due to glacial abrasion upstream) increased the flow of sediments delivered to the canyon heads (Baztan et al., 2005). Therefore, erosion by such currents formed the vertical and overhanging structures under which cold-water corals in Lacaze-Duthiers Canyon have mainly settled and developed. These structures were previously described as overhanging rocky walls (Fiala-Medioni et al., 2012; Gori et al., 2013; Fabri et al., 2014) but not as sub-parallel lithified sedimentary strata. The access to high resolution bathymetric data allowed reaching the scale of a community and mapping the extent of the habitat at a very local scale (see Fig. 10 for a global map). We calculated the slopes on the flanks of the canyon where we had high-resolution data, and followed the most prominent and outcropped sedimentary strata along the flanks of the canyons.

In addition to the outcropped strata, we were able to observe another type of habitat for cold-water corals, consisting of boulder fields presumably generated after rock avalanches from the collapse of overhanging strata on canyon walls, likely eroded and weakened by contemporary currents affecting the base of the cliffs. Moored oceanographic equipment at the head of the Lacaze-Duthiers Canyon revealed that near-bottom currents can reach up to 60 cm/s during regular dense shelf water cascading events (Ogston et al., 2008), and such strong currents can even reach deeper canyon regions (>1000 m water depth) during intense cascading events (Durrieu de Madron et al., 2011; Palanques et al., 2012). Presumably, the coral colonies previously described in the Lacaze-Duthiers Canyon as coral colonies growing in sedimented

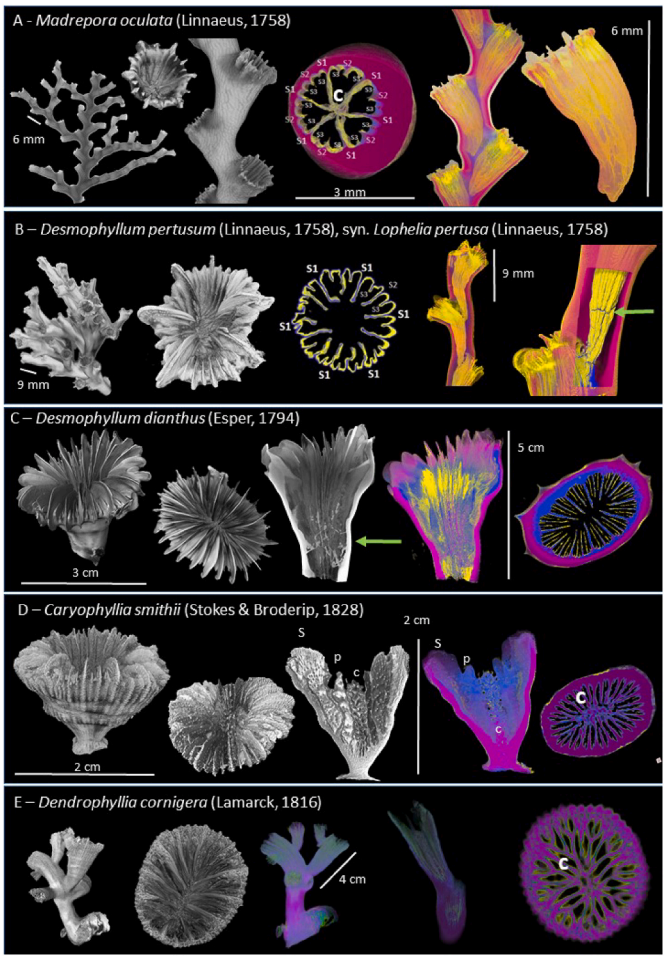

Fig. 9. Tomographic models of five scleractinian species found in the deep Mediterranean Sea. S: septa, p: pali; c: columella. Green arrows show thin internal horizontal structures in the basal part of calices of *Desmophyllum* genus. Density is represented in color, from high densities in pink, to blue and yellow for low densities. The images are not calibrated and the density values cannot be compared between samples.

areas further south in the canyon (Fiala-Medioni et al., 2012; Gori et al., 2013; Fabri et al., 2014) correspond to coral colonies living on top of eroded blocks.

Cold-water corals are generally observed as isolated colonies in canyons (Wienberg and Titschack, 2017). However, canyons are often vast and difficult to access so have not yet been extensively explored. Access to rugged environments with underwater robotic vehicles and a new application (45° angle) of a traditional (MBES) mapping technology makes it possible to discover new ecosystems hidden in unlikely places.

Canyons contiguous to Lacaze-Duthiers, in the western Gulf of Lion, such as Cap de Creus, La Fonera and Blanes canyons have been recently explored and described as hosting cold-water corals on their walls (Gori et al., 2013; Lastras et al., 2016; Lo Iacono et al., 2018; Santin et al., 2021). Generally, in the Mediterranean Sea, canyons are being increasingly explored, and new cold-water coral sites are described regularly, *i.e.* the Cassidaigne Canyon in the eastern Gulf of Lion (Fabri et al., 2019); the Levante canyon in the Ligurian Sea (Fanelli et al., 2017); the Dohrn canyon off Naples (Taviani et al., 2019); the Nora canyon off Sardinia (Taviani et al., 2017); and the Bari canyon in the Adriatic Sea (Angeletti et al., 2014). In the north-east Atlantic canyons are also found to be habitats for cold-water corals, for example, in the Bay of Biscay (van den Beld et al., 2017) or further north in the Whittard canyon, where a similar study using an inclined MBES on an ROV and photogrammetric models also evidenced highly complex topographic environments and vertical walls to be preferential habitats for coral populations (Robert et al., 2017). These cold-water ecosystems are composed of engineering species capable of sheltering a multitude of other species, and when they are close to the coasts, they often undergo anthropogenic pressures. It is our duty to identify their habitats and map them so that they can be protected in parks in which regulations can be enforced. New developments in submarine technologies, like the use of an MBES in an inclined position to map vertical structures, show great potential for describing new habitats for cold-water corals. The use of a similar configuration to that used for this study will be developed and probably lead to improvements in habitat mapping dedicated to canyons.

4.2. 3D-Reconstructions produced with photographic images for the coral assemblage scale (Photogrammetry)

The presence of coral colonies in the Lacaze-Duthiers Canyon has been known since the 1960s (Reyss, 1964), and has been subject to many studies (Fiala-Medioni et al., 2012; Gori et al., 2013; Lartaud et al., 2013, 2017b; Maier et al., 2013). However, our study sheds new light on cold-water coral distribution in this canyon using innovative techniques like photogrammetry, allowing accurate measurements to be taken in three dimensions. Underwater photogrammetry accuracy mostly depends on sensor resolution, the distance to the scene and navigation data quality (Istenič et al., 2019). Given the acquisition configuration of the H-ROV Ariane in our study, we can expect an accuracy around 1 cm.

We constructed 16 3D-models of approximately 300 m^2 each (from 54 to 619 m^2). These models are distributed over four locations, on the cliffs and flanks of the Lacaze-Duthiers Canyon, where colonies of cold-water coral (CWC) are found. 3D-models provide an overview of these CWC habitats at the local scale. This scale is larger than what is seen in the field of view of a camera and allows having an overview of a marine ecosystem cleaned of the turbidity and color attenuation that are inherent to the underwater environment (Arnaubec et al., 2015; Istenič et al., 2019). In addition, 3D-models are georeferenced in space and scaled, which means we have access to reliable and reproducible measurements. Repeated mapping is an effective tool for monitoring the temporal dynamics of coral habitats, both in relation to climate change and increasing human pressure (Lim et al., 2021). The ability to manage and protect marine habitats depends on detailed knowledge of the benthic ecosystem, including its state of health and signs of human impact (Buhl-Mortensen et al., 2015). Specific gaps in research knowledge have been identified, among which seabed mapping is frequently listed (Buhl-Mortensen et al., 2015). Using acoustic technologies such as hull-mounted multibeam echosounders, it is possible to acquire high-resolution, full-coverage imagery of the seafloor over extensive areas. In addition, visual inspection using an underwater video camera not only provides detailed information on the general features visible in multibeam data, they provide an excellent basis for biological investigation across a range of bottom types. However, the geomorphology of the seafloor imposes limitations on what type of video exploration can bring information. When bottoms are relatively flat, on cold-water coral mounds, 2D-mosaics are commonly used by the scientific community for habitat mapping, such as those on Porcupine Seabight, NE Atlantic (Lim et al., 2018). However, cold-water coral ecosystems are increasingly being reported in canyons where they are located on rocky outcrops and steep slopes (Fabri et al., 2014; Taviani et al., 2017; van den Beld et al., 2017; Aymà et al., 2019). Those rough environments provide shelter to cold-water coral communities (Puig and Gili, 2019) but are not suitable for 2D-mosaic techniques (Fabri et al., 2019). However, quantitative measurements are essential for mapping habitat extent and for implementing management and conservation programs (Danovaro et al., 2020). Thanks to advances in computer processing, the development of new techniques allowing 3D-reconstructions over large areas, offers new potential for scientific studies on structurally complex habitats (Lim et al., 2021).

3D-reconstructions in the Lacaze-Duthiers Canyon will be a testament to what we observed in 2019, and they will be a reference for future monitoring programs. These measurements have been used in an attempt to quantify the surfaces covered by vulnerable populations for the needs of the Marine Strategy Framework Directive (MFSD) (European Commission, 2008, 2017). The MSFD commits European Union (EU) Member States to implement 6-year monitoring and regulation cycles to reduce anthropogenic impacts with the aim of achieving the good environmental status (GES) of their marine waters by 2030 (Danovaro et al., 2020). Our study in the Lacaze-Duthiers Canyon is the first step to assess the spatial coverage of these cold-water corals considered Vulnerable Marine Ecosystem (VME) by several European organizations (OSPAR, 2010; FAO, 2016; GFCM, 2018).

4.2.1. Spatial and vertical distribution of both colonial coral species

Thanks to the photogrammetry technique we could create large mosaics of extensive vertical areas that we used to interpret the 3 dimensions of a scene in great detail. These techniques allowed placing individual visual observations within their direct spatial context instead of looking through the lens of a camera. Therefore, from our data, we can report that *D. pertusum* colonies cover surface areas of up to 100 m^2 at strategic places in the canyon, while *M.oculata* covers surface areas ranging from 100 to 600 m^2 along lithified sedimentary strata shown by fine scale bathymetry. We were able to document colonies aligned along strata up to 80 m long. The same values were reported from the mapping of vertical cliffs in Whittard canyon, NE Atlantic, with an MBES mounted on an AUV (Huvenne et al., 2011; Robert et al., 2017).

Previous studies in the same canyon, based on only 555 and 97 colonies of *M. oculata* and *D. pertusum* respectively, reported information from a larger range of depths (220 m–540 m depths) (Fiala-Medioni et al., 2012; Gori et al., 2013; Lartaud et al., 2017b) than we do (250 m–350 m depths). *M. oculata* was reported to be 10-fold more abundant than *D. pertusum,* which is what we found at dive locations 142–04 and 144–06. However, in some areas of the western flank, *M. oculata* was present in lower proportion, as it represented 70% and 85% of the coral population (Table 1), which means *M. oculata* was only 2.2 and 5.6-fold more abundant than *D. pertusum*.

A recent *in situ* study in the Lacaze-Duthiers Canyon focused on a transplant experiment between two sites (300 and 530 m depth) and on bacterial associations of both coral species, and concluded that *M. oculata* preferred shallower habitats whereas *D. pertusum* did not show such a preference (Lartaud et al., 2013; Chapron et al., 2020a). This is in line with the bathymetric distribution we observed in the canyon, where *M. oculata* was always seen at shallower depths than *D. pertusum*, but on dive 143–05 we found both species at similar depths (332 and 333m), although *M. oculata* was statistically deeper than *D. pertusum* simply because both species were located on the same stratum (Fig. 3), and all the *M. oculata* colonies were aligned slightly deeper than the *D. pertusum* colonies.

Our study is the first to show images of orange colonies of *D. pertusum* in the Lacaze-Duthiers Canyon. These large colonies were colored, but also thriving and mixed with white colonies. They formed groups of 2-m long bushes at 280 m depth (Fig. 4). This was an unexpected finding for two reasons: (1) *D. pertusum* was generally observed as isolated colonies in canyons of the Mediterranean Sea (Wienberg and Titschack, 2017); (2) coral mounds are thought to be the favored features on which thriving populations of *D. pertusum* would be found in the Mediterranean Sea (Savini et al., 2016; Corbera et al., 2019). However, these bushes of white and orange colonies in the canyon were thriving populations, and suggest that the orange color of the colonies is a sign of good health, but it could also be related to the quality of the organic matter they ingest. The orange color has already been described for *D. pertusum* colonies in canyons the Bay of Biscay in the Atlantic Ocean (Huvenne et al., 2011; van den Beld et al., 2017), but also on a Cabliers Coral Mound in the Alboran Sea (Corbera et al., 2019). We hypothesize that food quality is at the origin of the color of *D. pertusum* colonies.

4.2.2. Surface coverage and colony densities of both colonial coral species

We georeferenced 9503 coral colonies on an area of 4370 m^2 reconstructed in Lacaze-Duthiers Canyon, which gives a mean density of approximately 2.2 colonies per m^2 over 4500 m^2. The average densities of each species were 1.9 col./m^2 of *M.oculata* and 0.3 col./m^2 of *D. pertusum*, with maximum values up to 4 and 1.4 col./m^2, respectively. These values are higher than those reported in the contiguous Cap de Creus Canyon, where average densities were found to be up to 0.3 col./m^2 of *M.oculata* and up to 0.08 col./m^2 of *D. pertusum* (Orejas et al., 2009). In the Levante Canyon in the Ligurian Sea, *M. ocualata* show a mean density of 0.6 col./m^2, which is also lower than what we found, and no *D. pertusum* was seen there (Fanelli et al., 2017).

Colonies were not equally distributed and we found several areas on the western flank with colony densities exceeding 3 colonies per m^2. The maximum densities for both species were 4 colonies per m^2 over surfaces of around 100 m^2 for *D. pertusum*, and up to 600 m^2 for *M. oculata*. This diversity in colony densities at local scale depends on several factors such as the availability of a free hard substrate for larvae settlement (Strömberg and Larsson, 2017; Strömberg et al., 2019), food supply of organic matter, which depends on water currents (Palanques et al., 2006), but also seafloor characteristics such as slope, rugosity or aspect widely used in predictive habitat suitability models (Bargain et al., 2018). These environmental factors combined with biological ones such as reproduction strategies (Waller and Tyler, 2005; Pires et al., 2014) may lead to different spatial distributions for each coral species. Therefore detailed mapping is important and provides a measure of the habitat extent of each species, the first step toward ecosystem management (Buhl-Mortensen et al., 2015).

A location, described as a massive coral framework structure in the Lacaze-Duthiers Canyon, visited previously in 2009 during the Medseacan cruise and on which no measurement was performed (Gori et al., 2013), was explored on dive 143–05. With the 3D-models we built, we can now place in context the colonies seen in 2009 and understand that they were part of a bush around 2.5 m long, and that there were other bushes (Fig. 7) that had settled in a complex topographic area covering at least 250 m^2 on the western flank of the canyon (dive location 143–05, north face).

In the Cassidaigne Canyon, located on the eastern side of the Gulf of Lion, 33 photogrammetric models were built to evaluate the status of *M. oculata* populations at four locations in the canyon, (Fabri et al., 2019). Colonies were seen in higher density (9 colonies/m^2) under an overhang of around 300 m^2 on top of a wall. However, the colonies there were very small, with mean sizes ranging from 10 to 13 cm. Since they were upside down and coral rubble covered terraces below the overhang, it was assumed they had fallen due to their own weight and because of their downward orientation. Colonies would thus naturally be unable to reach a large size at this location (Fabri et al., 2019). On the main site, at a depth of 200 m, the *M. oculata* population having a mean density between 7 and 12 colonies/m^2 was restricted to small surfaces areas ranging from 3 to 9 m^2, with the largest knoll (n°3) showing 7 colonies/m^2 over 100 m^2. The location at a depth of 500 m in Cassidaigne Canyon was that which resembled most what we saw in the Lacaze-Duthiers Canyon, with a mean density of 4 colonies/m^2 over a surface area of 924 m^2, stretching along a rocky ledge.

The density values reported from several canyons of the Bay of Biscay, NE Atlantic, show lower densities of *M. oculata* and higher densities of *D. pertusum* than those in the Lacaze-Duthiers Canyon, with average densities of *M. oculata* and *D. pertusum* up to 1.64 and 0.69 col./m^2 respectively (Arnaud-Haond et al., 2017). Likewise, on Rockall bank (Logatchev mounds) off Ireland, where densities reached 1.04 and 1.41 col./m^2 respectively, whereas densities were lower on coral mounds off Iceland for both species (0.12 and 0.26 col./m^2) (Arnaud-Haond et al., 2017). And in SE Atlantic, on coral mounds off Angola, a recent study also reported average densities of *M. oculata* colonies with lower values than those in the Lacaze-Duthiers Canyon (0.53 col./m^2) (Orejas et al., 2021). On the contrary, on Cabliers Mound, described as the only known

coral mound province in the Mediterranean Sea with a currently growing reef, maximum values of coral density are higher than what we saw, up to 6 col./m^2 of *M. oculata* and 5 col./m^2 of *D. pertusum*, but average densities are lower with 0.81 and 0.14 col./m^2 respectively (Corbera et al., 2019).

The average densities of coral colonies in the Lacaze-Duthiers Canyon are the highest compared with what was found in other canyons of the Mediterranean Sea, and comparable to what was found on Cabliers mound in the Alboran Sea. Therefore, we assume canyons, like coral mounds, can be a place of development for thriving coral colonies. This is in line with a recent study in which submarine canyons have been identified as highly suitable areas for *D. pertusum* using ecological niche modeling (Matos et al., 2021).

4.2.3. Size structure of both colonial coral populations

Our measurements show an average height of the *D. pertusum* colonies (28 ± 15 cm) taller than that of *M. oculata* (18 ± 7 cm). The difference was even more obvious for maximum heights, reaching around 90 cm for *D. pertusum* and 50 cm for *M. oculata*. A previous study in the same canyon also reported large colonies for *D. pertusum* (diameter larger than 40 cm) and smaller ones for *M. oculata,* but larger *M. oculata* colonies were seen (diameter between 20 and 40 cm) at deeper zones (340 m) than at shallower ones (250 m) (diameter between 10 and 20 cm) (Gori et al., 2013). This is not in line with our results which reflect a uniform height distribution at the four locations we explored, which are in the same range of depths (250–340 m). The difference in size distribution between both studies in the Lacaze-Duthiers Canyon is probably due to (1) the size of datasets (555 colonies against 4536 colonies) and (2) the method used, as 3D reconstructions probably allow more accurate measurements than videos and laser beams. But, even if the colonies were seen in the same range of depths, they may not have been seen in the same range of slopes (cliff vs boulder). Colonies on vertical parts may break and fall under their own weight and thus their height can be limited there. Coral colony size may not be related to depths, but to slopes.

By comparison with other measurements carried out on coral colonies, we can see that *M. oculata* can exceed heights of 1 m, although we did not observe this in our study. In the Levante canyon, in the Ligurian Sea, the tallest colonies of *M. oculata* were measured and the maximum height was around 80–90 cm, with one colony of 100 cm height presented in a photo which shows a colony oriented upwards (Fanelli et al., 2017). In the SE Atlantic, on coral mounds off Angola, *M. oculata* colonies show average heights of 61 cm, with maximum up to 125 cm (oriented upwards) (Orejas et al., 2021). In our study, we explored the vertical parts of the canyon where colonies grow horizontally, implying that they may have difficulty supporting long branches; this could explain the difference in size compared to sites where colonies grow upward. On coral mounds off Angola (Orejas et al., 2021) coral colonies formed bushes like those we observed on our photogrammetric models, with smaller sizes (1.2 m) than those we measured in the canyon for *M. oculata* (1.8 m), and even smaller than the bushes formed by *D. pertusum* (2.5 m).

In our study, the size structure of the *M. oculata* population is similar at the four sites and is composed of 3 statistical groups, the largest group (53% of the population) is composed of colonies with an average height of 18 cm. The rest of the population is distributed in groups with mean heights of 12 cm and 27 cm. On the contrary, *D. pertusum* populations showed a different pattern in height distribution at each location. The head of the canyon (dives 142–04 and 144–06) had only small size colonies (mean height 16 cm). And on the contrary, on the western flank, where we encountered thriving colonies, populations harbor at least 2 statistical groups of large colonies (over 40% with mean heights of 26–28 cm and less than 30% with mean heights of 44–52 cm). These large colonies formed several bushes of 2.5 m long and can be seen at https://image.ifremer.fr/data/00746/85828/(Fabri et al., 2022a).

These size groups may be the result of inter-annual variability in environmental conditions induced by hydrological processes. A recent study showed that coral growth was different depending on episodic meteorological events and that episodic hydrological events inside the canyon, like dense shelf water cascading and winter storms, are likely to modulate the quality and quantity of food available for cold-water corals (Chapron et al., 2020b). High sedimentation rates and the transport of coarse sediments at the canyon head environments (Gaudin et al., 2006) can negatively impact the budding rate and linear extension because exposure to sediment limits access to food and oxygen for the polyp and leads to physical abrasion of the coral tissues. Thus, recurrent cascading events and severe winter storms can generate enhanced down canyon currents that prevent excessive sedimentation but may have a negative effect on linear extension, with the currents being too strong to allow polyps to catch their food (Chapron et al., 2020b). Therefore, the optimal growth for both species in the Lacaze-Duthiers canyon seems to be favored by episodic winter down canyon events of moderate intensity. However, both species may respond differently to moderate events, and while *D. pertusum* may present a linear extension, *M. oculata* may not follow the same pattern, because the quality of nutrients transported from surface to deeper areas depends on the time of year, thus providing different types of food supply. Also, *M. oculata* may be more sensitive than *D. pertusum* to environmental variations (Chapron et al., 2020b). Consequently, coral colony growth (budding rate and linear extension) differs between the two species and varies from year to year depending on the type of hydrological event (Chapron et al., 2020b). This could explain the different size distribution between the two species.

In addition, stronger episodic cascading events inside the canyon could induce strong current acceleration on the canyon seafloor, flushing coarse sediment particles (Canals et al., 2006; Palanques et al., 2012; Puig et al., 2012) that are likely to erode the sedimentary strata along the canyon flanks and may lead to the dislodging of blocks as was seen at the foot of the cliffs on the tributary canyon spurs. These eroded strata provide exposure of fresh hard substrates which are potentially attachment areas for coral larvae. Both species are believed to have different colonization strategies, with *M. oculata* producing multiple cohorts of gametes, thus taking advantage of every newly available ground, while *D. pertusum* may reproduce seasonally (Waller and Tyler, 2005; Pires et al., 2014). Therefore, the difference between size groups of both species evidenced by the statistics could be a consequence of the alternation of episodic events in the canyon, favoring food supply in case of moderate events, and the availability of free hard substrates in case of strong events, combined with the colonization strategy of each species.

Another study based on measurements from photogrammetric models was performed in the Cassidaigne Canyon in which only one cold-water coral species lives, *M. oculata* (Fabri et al., 2019). Generally, colonies of *M. oculata* were smaller in the Cassidaigne Canyon than in the Lacaze-Duthiers Canyon, with 60% of the population belonging to groups of small size colonies (6–9 cm and 10–16 cm). The surface of the area colonized by the species is also lower in the Cassidaigne Canyon (1650 m^2) than in the Lacaze-Duthiers Canyon (at least 4370 m^2 reconstructed in this study). Environmental conditions in the Lacaze-Duthiers Canyon may be more favorable to cold-water corals than those in the Cassidaigne Canyon, which can be explained by several factors: (1) the industrial wastes (bauxite residues) expelled in the Cassidaigne Canyon for more than 50 years might have reduced cold-water coral populations by suffocating them and by covering all the hard substrates, preventing larvae from settling (Fabri et al., 2017); (2) Cascading events occurring in the western canyons of the Gulf of Lion have already been described as generating dense costal and shelf waters exported down canyon (Palanques et al., 2006; Puig et al., 2008; Sanchez-Vidal et al., 2008, 2009; Ulses et al., 2008a, 2008b; Pasqual et al., 2010) and being decisive for coral populations (Chapron et al., 2020b); (3) storm induced downwelling events occurring in the western Gulf of Lion without involving cascading (Martín et al., 2013) might be also more favorable than the general upwelling occurring in the Cassidaigne

Canyon (Millot, 1990, 1999).

4.2.4. Coral colony orientations

Coral colonies were seen oriented northward along lithified sedimentary strata on the flanks of the canyon, and towards the east and west in gullies on either side of the axis (Fig. 7). Since cold-water corals rely on water currents for food, they adapt their morphology in response to environmental stressors, orienting branches in the main current direction (Sanna and Freiwald, 2021). In our study, coral colonies of both species faced prevailing currents coming from canyon head incisions.

Looking more precisely at the distribution of each species, we could observe that *D. pertusum* colonies settled at strategic locations on both flanks of the canyon. They were located at the spurs formed between the canyon flank tributaries and the main canyon axis, where the topography forms outgrowths on the canyon flanks (Fig. 10). Flows coming from both directions, along the main canyon and from the canyon head tributaries, can converge there, probably creating a local disturbance in the water column, which could be an element in favor of *D. pertusum* growth, particularly on the western flank, where the largest sizes of *D. pertusum* were observed.

Colonies of *M. oculata* were seen living around colonies of *D. pertusum* at these strategic places, as if they were at the periphery of a hot spot (Fig. 10, both dives on the western flank). We can hypothesize that competition between both species occurs regarding settlement at the best location (*i.e.* on the canyon flank spurs). We encountered mainly dense populations of *M. oculata* over large areas along lithified sedimentary strata in the main canyon axis, with almost no *D. pertusum*. In this part of the canyon, the current flow is probably more steady and unidirectional. Additionally, the continuous reproductive strategy of *M. oculata* to take advantage of any available hard substrate for larval colonization (Waller and Tyler, 2005) is likely an effective way to expand its spatial distribution in an unstable environment such as a canyon.

The north of the canyon, at dive location 142–04, harbored mainly *M. oculata* colonies along the lithified strata of the main wall (270 m depth). *Madrepora oculata* colonies did not show any particular orientation (east or west), which led us to think that the currents there came from both sides, east and west. At the foot of the cliff, colonies of *D. pertusum* were seen among *M. oculata* colonies, located on the blocks of a boulders field (320 m depth). Since the edge of the wall is so abrupt, there might be circulation vortexes behind the obstacle that might create a near-bottom recirculation from the down-canyon currents coming from the main canyon head. This local turbulence might also favor *D. pertusum* settlement in the boulder field.

In any case, the further away from complex topographic areas, the fewer coral colonies were observed.

4.2.5. Lost fishing gears

An evaluation of anthropogenic marine litter compiled at the European scale reported that the highest density occurs in submarine canyons, compared to seamounts, banks, continental shelves, continental slopes, and ocean ridges (Pham et al., 2014). In addition, litter density is reported to be at least 2 times more important in the Mediterranean Sea than in other European seas (Tubau et al., 2015).

The lost fishing gears seen in our study were longlines and nets, as often reported in canyon heads at water depths less than 500 m (Tubau et al., 2015). In the adjacent canyons (Cap Creus and La Fonera) lost fishing gear was evaluated to be 11% of the total marine litter (852 items seen along 32.7 km), which gives 2.8 fishing gears/km. This is in line with what was found in the Lacaze-Duthiers Canyon where fishing gear was previously reported with an average density of 3 items/km, which was the maximum observed among all the French continental canyons (Fabri et al., 2014). In this study we measured longline lengths on photogrammetric models and calculated the length found on the reconstructed surface. We found an overall density of 16 cm of longlines per m^2 over a surface of 4370 m^2 reconstructed at the head of the canyon. The highest density of longlines (30 cm per m^2) was seen on both flanks, at dive locations 143–05 and 144–06. Longlines were either entangled in coral colonies, or used as substratum, mainly by oysters (*Neopycnodonte cochlear*) but also by coral colonies, crinoids and polychetes. This density of longlines of 16 cm/m^2, although impressive, is under-evaluated for two reasons: (1) only colonized longlines could be reconstructed because very thin plastic strings could not be seen on videos or on 3D-models; (2) longlines are dangerous for ROV navigation, therefore they were avoided when seen during ROV dives in order to avoid being trapped by them.

During the CALADU cruise in October 2019, we met a Spanish longliner fishing boat, mooring its longline in the morning and recovering it in the afternoon, always at the same location on the western flank of the canyon. We located both ends of the longlines on our synthetic map, and it appeared along the western flank, stretching for 4 km, where lithified sedimentary strata were detected by HR bathymetry (slopes >50%) (Fig. 10). The fisherman arrived early in the morning, every day except Sunday, which prevented us several times from diving with the ROV on the western flank for security reasons. This flank of the canyon was (1) either the closest site from its home port, or (2) a very productive fishing site. We think that the western flank of the canyon, with its thriving communities of cold-water corals providing shelter, food and a breeding ground for various species, has long attracted fishermen as well.

In addition, we also observed 4 nets covering a total surface area of 227 m^2. A few times nets were seen to be used as substrate by oysters (*N. cochlear*). No direct harm on organisms was observed, however no coral colonies were seen settled on the nets.

In the context of the MFSD (European Commission, 2008), one of the descriptors of ecosystem status is the measurement of anthropogenic impact, reporting on the number of species adversely affected by marine litter. With regard to vulnerable cold-water coral ecosystems, although we did not count the number of colonies entangled in longlines, we can report that there were longlines everywhere. We can hardly find an image without a piece of longline in the Lacaze-Duthiers Canyon. If we try to draw a parallel with what a terrestrial ecosystem would look like with a level of pollution similar to what we have seen underwater, it would be intolerable. As already reported, longlines are harmful at the time of impact with colonies because they can be broken, either during hauling or during recovery. If the line gets trapped in the coral structures, the longliner in its attempt to encircle the site to disentangle the line, may cause damage or destruction to the habitat (Ragnarsson et al., 2017). But once the longline is lost for the fisherman, it becomes an artificial substrate on which many species can grow (Tubau et al., 2015).

We regret that even if the Lacaze-Duthiers Canyon has been located in the marine park of the Gulf of Lion since 2011 (Fabri et al., 2014), regulations do not exist on fishing practices ten years after its creation.

4.3. 3D-Reconstructions produced with radiographic data for the coral species scale (Micro-computed tomography)

Micro-computed tomography (micro-CT) and three-dimensional (3D) visualization techniques have become an increasingly popular tool used in many fields of life science, especially in taxonomy (Faulwetter et al., 2013). The advantage of this imaging technique lies in its power to construct high-resolution, cross-sectional views of skeletons without causing damage during the analysis. The five scleractinian species found in the Lacaze-Duthiers Canyon, called “stony corals” because of their external calcified skeleton, were ideal candidates for this internal inspection using X-rays.

Scleractinian corals form 3D-structures that provide various ecological niches for associated fauna and therefore are called “ecosystem engineers” or “Deep-water Reef-forming corals” thanks to their skeleton (Rogers, 1999). The skeletal growth of calcifying species occurs through the periodic addition of carbonate, but also by the addition of new polyps at the apex of each branch of the colony (Lartaud

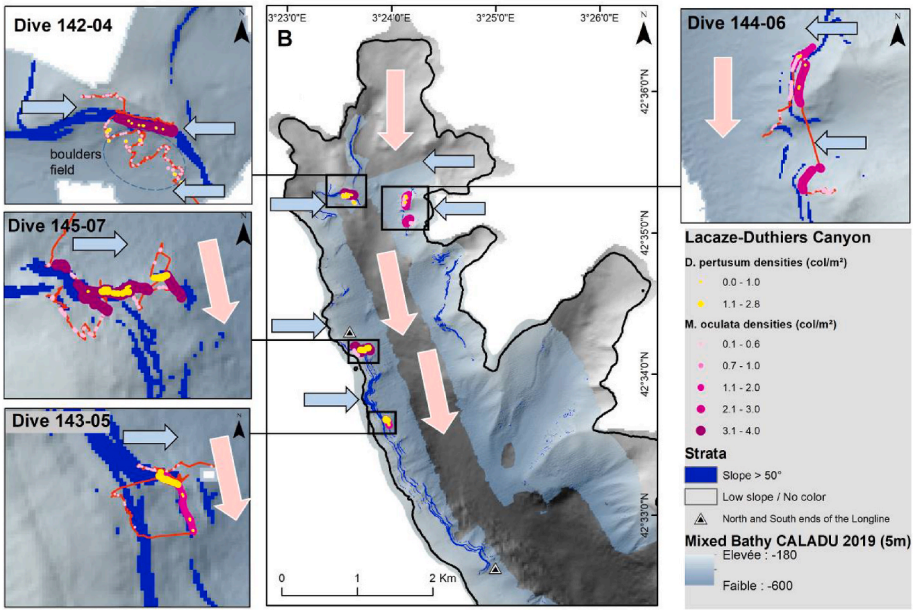

Fig. 10. Global map of the head of the Lacaze-Duthiers Canyon gathering all the information deduced from 3D representations. Lithified sedimentary strata (evidenced by slopes >50°) are represented in blue; Coral colonies of *M. oculata* and *D. pertusum* are reported as pink and yellow dots, respectively. Blue and black arrows show current flows deduced from 3D-representations; pink and white arrows show the prevailing current. High resolution bathymetry is a mix of Hull-mounted and Ariane MBES data.

et al., 2017b). The communication between each polyp of a scleractinian colony (tropical and cold species) is external, through the soft tissue (ceonosarc) covering the skeleton. However, the comparison between the skeletons of *D. pertusum* and *M. oculata*, showed that calices of successive generations were connected by a thin canal in the *D. pertusum* skeleton but not in the *M. oculata* skeleton (Fig. 9). This is in agreement with a recent complementary study performed by the dissolution of calcified skeletons, which reveals soft tissues connecting two polyps living in successive calices (Lartaud et al., 2019). Both species are composed, among other things, of the ceonosarc covering the skeleton, but only *D. pertusum* harbors mesenterial filaments connecting polyps inside the skeleton (Lartaud et al., 2019; Mouchi et al., 2019). In our study we observed that *D. pertusum* coral colonies can build 3D skeletons higher than *M. oculata* ones (1 m and 0.5 m). The reason could be that the skeleton built by *D. pertusum* might be higher due to the presence of these thin canals connecting calices, allowing (1) efficient communication between polyps, (2) a protected communication with regard to external attacks. This would allow *D. pertusum* to better develop its skeleton over time, which *M. oculata* cannot do.

The skeleton of these organisms is dedicated to colony structure, and the protection of soft tissues against predators and chemical threats (Lartaud et al., 2017b). Cold-water corals produce carbonate growth increments, and due to their growth by the addition of new polyps, the radial cross-section of a branch corresponds to the radial cross-section of a polyp, and therefore reflects only a small part of the colony's growth history (Lartaud et al., 2017a). In addition, two growth centers were revealed by staining experiments, one on the outer edge of a calyx and another one on the inner edge near the septa (Lartaud et al., 2013). On our micro-CT scans, we can identify the densest areas (pink) that bear most of the mechanical loads due to the weight of the colony and allow resisting water currents, whereas less dense areas (yellow) are dedicated to the protection and support of the polyps (internal organization). We also observed material of intermediate density (blue) inside the dense skeleton, where a calyx is inserted over the previous one. This intermediate density skeleton could be due to the complex bi-directional growth structures described previously (Gass and Roberts, 2011; Lartaud et al., 2013), and be attributed to polyp producing growth increments both inside and outside the calyx.

By comparing two species of the genus *Desmophyllum*, a colonial (*D. pertusum*) and a solitary species (*D. dianthus*) with the micro-CT technique, we were able to observe that the genus *Desmophyllum* lacks pali and columella as already described in a genetic study merging the two species into the genus *Desmophyllum* (Addamo et al., 2016). We were also able to observe the presence of thin horizontal structures in both species at the bottom of calices. These skeletal structures were referred to as *dissepiment* or *tabulae* in a study describing *D. dianthus* in detail (Lazier et al., 1999). No function has been attributed to these horizontal structures, and they do not prevent communication between calices because they exist only between contiguous septa and do not cross the calyx from side to side, so they might exist to consolidate series of vertical septa.

Because of their long lifespan and calcified skeletons, deep-sea corals have long been examined to identify possible patterns that could reveal a chronology for paleoceanographic reconstruction (Lazier et al., 1999; Risk et al., 2002). Growth bands were observed on different parts of their skeletons (septa and outer theca) after being sliced and examined in reflected light or with a scanning electron microscope (SEM) (Lazier et al., 1999; Risk et al., 2002; Adkins et al., 2004; Gass and Roberts, 2011; Lartaud et al., 2013). Using the micro-CT technique, growth bands in the theca wall of *D. pertusum* skeletons were clearly seen but on a smaller sample than those used in our study (pers. comm. X. de la Bernardie). The 3D representations we produced in this study have minimum voxel sizes of 9 and 10 μm and did not allow us to clearly see the growth bands. Indeed, to highlight the density bands it would be necessary to subsample the specimen, *i.e.* separate a septa from the individual or cut a piece of theca, in order to obtain a closer view of the samples in X-ray scans. A definition close to 4 μm could then be reached, which is necessary to highlight (1) growth bands that have been previously described and are less than 100 μm thick (Lazier et al., 1999; Mouchi et al., 2017), and (2) calcification centers or areas of rapid accretion deposition constituting growth bands that can be observed using electron backscatter diffraction in *D. pertusum* (Mouchi et al., 2017).

Our 3D-representations of a whole corallite or a piece of a colony have definitions ranging from 9 to 58 μm voxel size and allow observing taxonomic criteria. Videos of each species are available on https://image.ifremer.fr/data/00745/85674/(Fabri et al., 2022b). Morphological characteristics useful for identifying Scleractinia species (Zibrowius, 1980; Cairns and Kitahara, 2012; Altuna and Poliseno, 2019) are easily identified using micro-CT without sectioning the samples.

Micro-CT is a technique previously used for the identification of fossils because it allows the 3D visualization of calcified organisms that

have become stones (Reid et al., 2018). *Desmophyllum pertusum* has already been observed using micro-CT to visualize its response to bio-eroding sponge infestation, but not for its taxonomic characteristics (Beuck et al., 2007).This technique has also been used successfully for the description of a new species of marine invertebrate, a crustacean decapod (Landschoff et al., 2018) and to examine foraminiferan tests (Gooday et al., 2018), but was proven not so useful for soft-bodied invertebrates such as polychaetas (Paterson et al., 2014). Micro-CT was also considered to quantify the effect of ocean acidification on the calcareous skeletons of octocorallians (Enochs et al., 2015) and foraminiferans (Iwasaki et al., 2015). 3D-reconstructions of specimens produced by micro-CT will potentially be part of museum collections and will be a support for taxonomic research (Faulwetter et al., 2013).

5. Conclusions

3D-representations of bathymetric data obtained using an inclined MBES allowed mapping vertical walls and locating overhangs that are privileged coral habitats in canyons. We observed two habitats for cold-water corals in the Lacaze-Duthiers canyon, sedimentary strata and boulder fields formed by the collapse of overhanging strata.

3D-representations of ecosystems using photogrammetry techniques were used to measure quantitative parameters for populations. We measured (1) proportions, and found that *D. pertusum* comprised up to 31% of the coral population; (2) depths distribution, and found that *M. oculata* was mostly seen at shallower depths than *D. pertusum*; (3) size structure, and observed a uniform and heterogeneous distribution for *M. oculata* and *D. pertusum*, respectively, when comparing the four locations; (4) densities, and found that the average densities of coral colonies were the highest compared with what was found in other canyons of the Mediterranean Sea, and comparable to what was found on Cabliers mound in the Alboran Sea. The coral colonies faced the prevailing currents and we deduced the current flows from their orientation. Surfaces covered by pristine ecosystems and surfaces of the ecosystems adversely affected by anthropogenic impacts can be calculated. The lost fishing gears seen in our study were longlines and nets, with an overall density of 16 cm of longlines per m^2, up to 30 cm per m^2, over a surface of 4370 m^2. The photogrammetry technique also allowed preserving a 3D image of an ecosystem as a whole and will give the opportunity of monitoring its evolution through time by returning to the area at regular intervals, as requested by certain European directives like the Marine Framework Strategy Directive (6-year interval).

3D-representations of specimens using micro-CT allowed analyzing the morphological characteristics of species and visualizing internal parts at will to obtain transversal and longitudinal sections. The comparison between the skeletons of *D. pertusum* and *M. oculata*, showed that calices of successive generations were connected by a thin canal in the *D. pertusum* skeleton but not in the *M. oculata* skeleton. This technique can also be used to acquire information on skeleton densities without damaging the specimen. 3D models of specimens can be archived in the collections of Natural History Museums and provide another dimension for taxonomy. Thus, models can be shared with everyone, unlike physical specimens preserved in museums today.

Declaration of competing interest

The authors declare that they have no known competing financial interests or personal relationships that could have appeared to influence the work reported in this paper.

Data availability

Data will be made available on request.

Acknowledgements

This paper was written in the framework of the IDEM European project (Implementation of the second cycle of the marine strategy framework directive www.msfd-idem.eu) No. 11.0661/2017/750680/SUB/ENV.C2 and the Spanish research project ABRIC (Ref. RTI2018-096434-B-I00). We are grateful to all the participants of the CALADU cruise in 2019 (https://doi.org/10.17600/18000929). Furthermore we are indebted to Keith Hodson (http://www.accent-europe.fr) for correcting the English. The authors also thank the reviewers for their helpful comments aimed at improving the manuscript.

References

Addamo, A.M., Vertino, A., Stolarski, J., García-Jiménez, R., Taviani, M., Machordom, A., 2016. Merging scleractinian genera: the overwhelming genetic similarity between solitary *Desmophyllum* and colonial *Lophelia*. BMC Evol. Biol. 16 (1), 108. https://doi.org/10.1186/s12862-016-0654-8.

Addinsoft, 2019. XLSTAT Statistical and Data Analysis Solution.

Adkins, J.F., Henderson, G.M., Wang, S.L., O'Shea, S., Mokadem, F., 2004. Growth rates of the deep-sea scleractinia Desmophyllum cristagalli and Enallopsammia rostrata. Earth Planet Sci. Lett. 227 (3–4), 481–490. https://doi.org/10.1016/j.epsl.2004.08.022.

Altuna, A., Poliseno, A., 2019. 14 taxonomy, genetics and biodiversity of mediterranean deep-sea corals and cold-water corals. In: Orejas, C., Jiménez, C. (Eds.), Mediterranean Cold-Water Corals: Past, Present and Future: Understanding the Deep-Sea Realms of Coral. Springer International Publishing, Cham, pp. 121–156. https://doi.org/10.1007/978-3-319-91608-8_14.

Angeletti, L., Taviani, M., Canese, S., Foglini, F., Mastrototaro, F., Argnani, A., Trincardi, F., Bakran-Petricioli, T., Ceregato, A., Chimienti, G., et al., 2014. New deep-water cnidarian sites in the southern Adriatic Sea. Mediterr. Mar. Sci. 15 (2), 263–273. https://doi.org/10.12681/mms.558.

Arnaubec, A., Escartin, J., Opderbecke, J., Matabos, M., Gracias, N., in prep. Underwater 3D terrain reconstruction from video or still imagery: Processing and exploitation software (Matisse & 3DMetrics). https://github.com/IfremerUnderwater.

Arnaubec, A., Opderbecke, J., Allais, A.G., Brignone, L., 2015. Optical mapping with the ARIANE HROV at IFREMER: the MATISSE processing tool, OCEANS 2015 - genova, 18-21 May 2015. https://doi.org/10.1109/OCEANS-Genova.2015.7271713, 1-6.

Arnaud-Haond, S., Van den Beld, I.M.J., Becheler, R., Orejas, C., Menot, L., Frank, N., Grehan, A., Bourillet, J.F., 2017. Two "pillars" of cold-water coral reefs along Atlantic European margins: prevalent association of Madrepora oculata with Lophelia pertusa, from reef to colony scale. Deep Sea Res. Part II Top. Stud. Oceanogr. 145 (Suppl. C), 110–119. https://doi.org/10.1016/j.dsr2.2015.07.013.

Aymà, A., Aguzzi, J., Canals, M., Company, J.B., Lastras, G., Mecho, A., Lo Iacono, C., 2019. 26 occurrence of living cold-water corals at large depths within submarine canyons of the northwestern Mediterranean Sea. In: Orejas, C., Jiménez, C. (Eds.), Mediterranean Cold-Water Corals: Past, Present and Future: Understanding the Deep-Sea Realms of Coral. Springer International Publishing, Cham, pp. 271–284. https://doi.org/10.1007/978-3-319-91608-8_26.

Bargain, A., Foglini, F., Pairaud, I., Bonaldo, D., Carniel, S., Angeletti, L., Taviani, M., Rochette, S., Fabri, M.C., 2018. Predictive habitat modeling in two Mediterranean canyons including hydrodynamic variables. Prog. Oceanogr. https://doi.org/10.1016/j.pocean.2018.02.015.

Baztan, J., Berne, S., Olivet, J.L., Rabineau, M., Aslanian, D., Gaudin, A., Rehault, J.P., Canals, M., 2005. Axial incision: the key to understand submarine canyon evolution (in the western Gulf of Lion). Mar. Petrol. Geol. 22 (6–7), 805–826. https://doi.org/10.1016/j.marpetgeo.2005.03.011.

Berné, S., Gorini, C., 2005. The Gulf of Lions: an overview of recent studies within the French 'Margins' programme. Mar. Petrol. Geol. 22 (6–7), 691–693. https://doi.org/10.1016/j.marpetgeo.2005.04.004.

Berné, S., Loubrieu, B., equipe, Calmar, 1999. Canyons and recent sedimentary processes on the western Gulf of Lions margin. First results of the Calmar cruise. In: Comptes Rendus De l'Academie des sciences Serie II Fascicule a-Sciences de la Terre et des Planètes, 328, pp. 471–477. https://doi.org/10.1016/S1251-8050(99)80148-7, 7.

Beuck, L., Vertino, A., Stepina, E., Karolczak, M., Pfannkuche, O., 2007. Skeletal response of *Lophelia pertusa* (Scleractinia) to bioeroding sponge infestation visualised with micro-computed tomography. Facies 53 (2), 157–176. https://doi.org/10.1007/s10347-006-0094-9.

Buhl-Mortensen, L., Buhl-Mortensen, P., Dolan, M.J.F., Gonzalez-Mirelis, G., 2015. Habitat mapping as a tool for conservation and sustainable use of marine resources: some perspectives from the MAREANO Programme, Norway. J. Sea Res. 100, 46–61. https://doi.org/10.1016/j.seares.2014.10.014.

Buhl-Mortensen, L., Vanreusel, A., Gooday, A.J., Levin, L.A., Priede, I.G., Buhl-Mortensen, P., Gheerardyn, H., King, N.J., Raes, M., 2010. Biological structures as a source of habitat heterogeneity and biodiversity on the deep ocean margins. Mar. Ecol. Evolution. Perspect. 31 (1), 21–50. https://doi.org/10.1111/j.1439-0485.2010.00359.x.

Cairns, S.D., Kitahara, M.V., 2012. An illustrated key to the genera and subgenera of the Recent azooxanthellate Scleractinia (Cnidaria, Anthozoa), with an attached glossary. ZooKeys 227, 1–47. https://doi.org/10.3897/zookeys.227.3612.

Canals, M., Puig, P., Durrieu de Madron, X., Heussner, S., Palanques, A., Fabres, J., 2006. Flushing submarine canyons. Nature 444, 354–357. https://doi.org/10.1038/nature05271, 7117.

Chapron, L., Galand, P.E., Pruski, A.M., Peru, E., Vetion, G., Robin, S., Lartaud, F., 2021. Resilience of cold-water coral holobionts to thermal stress. Proc. Biol. Sci. 288, 1965. https://doi.org/10.1098/rspb.2021.2117.

Chapron, L., Lartaud, F., Le Bris, N., Peru, E., Galand, P.E., 2020a. Local variability in microbiome composition and growth suggests habitat preferences for two reef-building cold-water coral species. Front. Microbiol. 11 https://doi.org/10.3389/fmicb.2020.00275.

Chapron, L., Le Bris, N., Durrieu de Madron, X., Peru, E., Galand, P.E., Lartaud, F., 2020b. Long term monitoring of cold-water coral growth shows response to episodic meteorological events in the NW Mediterranean. Deep Sea Res. Oceanogr. Res. Pap. 160, 103255 https://doi.org/10.1016/j.dsr.2020.103255.

Corbera, G., Lo Iacono, C., Gràcia, E., Grinyó, J., Pierdomenico, M., Huvenne, V.A.I., Aguilar, R., Gili, J.M., 2019. Ecological characterisation of a mediterranean cold-water coral reef: Cabliers coral mound province (Alboran Sea, western mediterranean). Prog. Oceanogr. 175, 245–262. https://doi.org/10.1016/j.pocean.2019.04.010.

Danovaro, R., Fanelli, E., Canals, M., Ciuffardi, T., Fabri, M.C., Taviani, M., Argyrou, M., Azzurro, E., Bianchelli, S., Cantafaro, A., et al., 2020. Towards a marine strategy for the deep Mediterranean Sea: analysis of current ecological status. Mar. Pol. 112, 103781 https://doi.org/10.1016/j.marpol.2019.103781.

Dennielou, B., Jallet, L., Sultan, N., Jouet, G., Giresse, P., Voisset, M., Berne, S., 2009. Post-glacial persistence of turbiditic activity within the Rhone deep-sea turbidite system (Gulf of Lions, Western Mediterranean): linking the outer shelf and the basin sedimentary records. Mar. Geol. 257 (1–4), 65–86. https://doi.org/10.1016/j.margeo.2008.10.013.

du Plessis, A., Broeckhoven, C., Guelpa, A., le Roux, S.G., 2017. Laboratory x-ray micro-computed tomography: a user guideline for biological samples. GigaScience 6, 6. https://doi.org/10.1093/gigascience/gix027.

Durrieu de Madron, X., Abassi, A., Heussner, S., Monaco, A., Aloisi, J.C., Radakovitch, O., Giresse, P., Buscail, R., Kerherve, P., 2000. Particulate matter and organic carbon budgets for the Gulf of Lions (NW Mediterranean). Oceanol. Acta 23 (6), 717–730.

Durrieu de Madron, X., Guieu, C., Sempéré, R., Conan, P., Cossa, D., D'Ortenzio, F., Estournel, C., Gazeau, F., Rabouille, C., Stemmann, L., et al., 2011. Marine ecosystems' responses to climatic and anthropogenic forcings in the Mediterranean. Prog. Oceanogr. 91 (2), 97–166. https://doi.org/10.1016/j.pocean.2011.02.003.

Durrieu de Madron, X., Radakovitch, O., Heussner, S., Loye-Pilot, M.D., Monaco, A., 1999. Role of the climatological and current variability on shelf-slope exchanges of particulate matter: evidence from the Rhone continental margin (NW Mediterranean). Deep-Sea Res. I 46 (9), 1513–1538. https://doi.org/10.1016/S0967-0637(99)00015-1.

Durrieu de Madron, X., Zervakis, V., Theocharis, A., Georgopoulos, D., 2005. Comments on "Cascades of dense water around the world ocean". Prog. Oceanogr. 64 (1), 83–90. https://doi.org/10.1016/j.pocean.2004.08.004.

Enochs, I.C., Manzello, D.P., Wirshing, H.H., Carlton, R., Serafy, J., 2015. Micro-CT analysis of the Caribbean octocoral Eunicea flexuosa subjected to elevated pCO2. ICES (Int. Counc. Explor. Sea) J. Mar. Sci. 73 (3), 910–919. https://doi.org/10.1093/icesjms/fsv159.

European Commission, 2008. Council Regulation (EC 734/2008) on the protection of vulnerable marine ecosystems in the high seas from the adverse impacts of bottom fishing gears. Off. J. Eur. Union. www.eur-lex.europa.eu.

European Commission, 2017. Directive (EU) 2017/845 amending Directive 2008/56/EC of the European Parliament and of the Council as regards the indicative lists of elements to be taken into account for the preparation of marine strategies. Off. J. Eur. Union 27–33. http://data.europa.eu/eli/dir/2017/845/oj.

Fabri, M.-C., Arnaubec, A., Autin, T., Dugornay, O., 2022a. Traveling video in a 3D representation of cold-water coral assemblage (Photogrammetry). https://doi.org/10.24351/85828.

Fabri, M.-C., de La Bernardie, X., Dugornay, O., 2022b. Videos into the skeletons of five scleractinian species (micro-computed Tomography). https://doi.org/10.24351/85674.

Fabri, M.-C., Guerin, C., Piasco, R., Puig, P., 2022c. Fly-through video showing sharp bathymetric structures in the Lacaze-Duthiers Canyon. https://doi.org/10.24351/85829.

Fabri, M.-C., Vinha, B., Allais, A.-G., Bouhier, M.-E., Dugornay, O., Gaillot, A., Arnaubec, A., 2019. Evaluating the ecological status of cold-water coral habitats using non-invasive methods: an example from Cassidaigne canyon, northwestern Mediterranean Sea. Prog. Oceanogr. 178, 102172 https://doi.org/10.1016/j.pocean.2019.102172.

Fabri, M.C., Bargain, A., Pairaud, I., Pedel, L., Taupier-Letage, I., 2017. Cold-water coral ecosystems in Cassidaigne Canyon: an assessment of their environmental living conditions. Deep Sea Res. Part II Top. Stud. Oceanogr. 137, 436–453. https://doi.org/10.1016/j.dsr2.2016.06.006.

Fabri, M.C., Pedel, L., Beuck, L., Galgani, F., Hebbeln, D., Freiwald, A., 2014. Megafauna of vulnerable marine ecosystems in French mediterranean submarine canyons: spatial distribution and anthropogenic impacts. Deep Sea Res. Part II Top. Stud. Oceanogr. 104, 184–207. https://doi.org/10.1016/j.dsr2.2013.06.016.

Fanelli, E., Delbono, I., Ivaldi, R., Pratellesi, M., Cocito, S., Peirano, A., 2017. Cold-water coral Madrepora oculata in the eastern Ligurian Sea (NW mediterranean): historical and recent findings. Aquat. Conserv. Mar. Freshw. Ecosyst. 1–11. https://doi.org/10.1002/aqc.2751.

FAO, 2016. Vulnerable Marine Ecosystems : Processes and Practices in the High Seas. FAO Fisheries and Aquaculture Technical Paper No. 595. www.fao.org/3/a-i5952e.pdf.

Faulwetter, S., Vasileiadou, A., Kouratoras, M., Dailianis, T., Arvanitidis, C., 2013. Micro-computed tomography: introducing new dimensions to taxonomy. ZooKeys 263, 1–45. https://doi.org/10.3897/zookeys.263.4261.

Fiala-Medioni, A., Madurell, T., Romans, P., Reyss, D., Pibot, A., Watremez, P., Ghiglione, M., Ferrari, B., Vuillemin, R., Lebaron, P., et al., 2012. ROV and submersible surveys on faunal assemblages in a deep-sea canyon (Rech Lacaze-Duthiers, Western Mediterranean Sea). Vie Et Milieu-Life Environ. 62 (4), 173–190.

Freiwald, A., Beuck, L., Rüggeberg, A., Taviani, M., Hebbeln, D., 2009. The white coral community in the Central Mediterranean Sea revealed by ROV Surveys. Oceanography 22 (1), 58–74. https://doi.org/10.5670/oceanog.2009.06.

Galand, P.E., Chapron, L., Meistertzheim, A.L., Peru, E., Lartaud, F., 2018. The effect of captivity on the dynamics of active bacterial communities differs between two deep-sea coral species. Front. Microbiol. 9 https://doi.org/10.3389/fmicb.2018.02565.

Galand, P.E., Remize, M., Meistertzheim, A.L., Pruski, A.M., Peru, E., Suhrhoff, T.J., Le Bris, N., Vetion, G., Lartaud, F., 2020. Diet shapes cold-water corals bacterial communities. Environ. Microbiol. 22 (1), 354–368. https://doi.org/10.1111/1462-2920.14852.

Gass, S.E., Roberts, J.M., 2011. Growth and branching patterns of lophelia pertusa (scleractinia) from the north sea. J. Mar. Biol. Assoc. U. K. 91 (4), 831–835. https://doi.org/10.1017/S002531541000055X.

Gaudin, M., Berne, S., Jouanneau, J.M., Palanques, A., Puig, P., Mulder, T., Cirac, P., Rabineau, M., Imbert, P., 2006. Massive sand beds attributed to deposition by dense water cascades in the Bourcart canyon head, Gulf of Lions (northwestern Mediterranean Sea). Mar. Geol. 234 (1–4), 111–128. https://doi.org/10.1016/j.margeo.2006.09.020.

GFCM, 2018. Report of the Second Meeting of the Working Groups on Vulnerable Marine Ecosystems (WGVME), Feb. 2018. Working Group on Vulnerable Marine Ecosystems (WGVME). FAO, 57p. http://www.fao.org/gfcm/reports/technical-meetings/detail/en/c/1142043/.

Gooday, A.J., Sykes, D., Góral, T., Zubkov, M.V., Glover, A.G., 2018. Micro-CT 3D imaging reveals the internal structure of three abyssal xenophyophore species (Protista, Foraminifera) from the eastern equatorial Pacific Ocean. Sci. Rep. 8 (1), 12103. https://doi.org/10.1038/s41598-018-30186-2.

Gori, A., Orejas, C., Madurell, T., Bramanti, L., Martins, M., Quintanilla, E., Marti-Puig, P., Lo Iacono, C., Puig, P., Requena, S., et al., 2013. Bathymetrical distribution and size structure of cold-water coral populations in the Cap de Creus and Lacaze-Duthiers canyons (northwestern Mediterranean). Biogeosciences 10 (3), 2049–2060. https://doi.org/10.5194/bg-10-2049-2013.

Huvenne, V.A.I., Tyler, P.A., Masson, D.G., Fisher, E.H., Hauton, C., Huehnerbach, V., Le Bas, T.P., Wolff, G.A., 2011. A Picture on the wall: innovative mapping reveals cold-water coral refuge in submarine canyon. PLoS One 6 (12), e28755. https://doi.org/10.1371/journal.pone.0028755.

Istenič, K., Gracias, N., Arnaubec, A., Escartín, J., Garcia, R., 2019. Scale Accuracy evaluation of image-based 3D reconstruction strategies using laser photogrammetry. Rem. Sens. 11, 18. https://doi.org/10.3390/rs11182093.

Iwasaki, S., Kimoto, K., Sasaki, O., Kano, H., Honda, M.C., Okazaki, Y., 2015. Observation of the dissolution process of Globigerina bulloides tests (planktic foraminifera) by X-ray microcomputed tomography. Paleoceanography 30 (4), 317–331. https://doi.org/10.1002/2014PA002639.

Landschoff, J., Komai, T., du Plessis, A., Gouws, G., Griffiths, C.L., 2018. MicroCT imaging applied to description of a new species of Pagurus Fabricius, 1775 (Crustacea: Decapoda: anomura: Paguridae), with selection of three-dimensional type data. PLoS One 13 (9), e0203107. https://doi.org/10.1371/journal.pone.0203107.

Lartaud, F., Galli, G., Raza, A., Priori, C., Benedetti, M.C., Cau, A., Santangelo, G., Iannelli, M., Solidoro, C., Bramanti, L., 2017a. Growth patterns in long-lived coral species. In: [Rossi, S., Bramanti, L., Gori, A., Orejas, C. (Eds.), Marine Animal Forests: the Ecology of Benthic Biodiversity Hotspots. Springer International Publishing, Cham, pp. 595–626. https://doi.org/10.1007/978-3-319-21012-4_15.

Lartaud, F., Meistertzheim, A.L., Peru, E., Le Bris, N., 2017b. In situ growth experiments of reef-building cold-water corals: the good, the bad and the ugly. Deep-Sea Res. Part I Oceanogr. Res. Pap. 121, 70–78. https://doi.org/10.1016/j.dsr.2017.01.004.

Lartaud, F., Mouchi, V., Chapron, L., Meistertzheim, A.L., Le Bris, N., 2019. 36 growth patterns of mediterranean calcifying cold-water corals. In: Orejas, C., Jiménez, C. (Eds.), Mediterranean Cold-Water Corals: Past, Present and Future. Springer, Cham. https://doi.org/10.1007/978-3-319-91608-8_36.

Lartaud, F., Pareige, S., de Rafelis, M., Peuillassier, L., Bideau, M., Peru, E., Romans, P., Alcala, F., Le Bris, N., 2013. A new approach for assessing cold-water coral growth in situ using fluorescent calcein staining. Aquat. Living Resour. 26 (2), 187–196. https://doi.org/10.1051/alr/2012029.

Lastras, G., Canals, M., Ballesteros, E., Gili, J.M., Sanchez-Vidal, A., 2016. Cold-water corals and anthropogenic impacts in La Fonera submarine canyon head, northwestern Mediterranean Sea. PLoS One 11, 5. https://doi.org/10.1371/journal.pone.0155729.

Latief, F.D.E., Sari, D., Fitri, L.A., 2017. Applications of Micro-CT scanning in medicine and dentistry: microstructural analyses of a Wistar Rat mandible and a urinary tract stone. IOP Conf. Series: J. Phys. Conf. 884 https://doi.org/10.1088/1742-6596/884/1/012042.

Lazier, A.V., Smith, J.E., Risk, M.J., Schwarcz, H.P., 1999. The skeletal structure of Desmophyllum cristagalli: the use of deepwater corals in sclerochronology. Lethaia 32 (2), 119–130.

Lim, A., Kane, A., Arnaubec, A., Wheeler, A.J., 2018. Seabed image acquisition and survey design for cold water coral mound characterisation. Mar. Geol. 395, 22–32. https://doi.org/10.1016/j.margeo.2017.09.008.

Lim, A., Wheeler, A.J., Conti, L., 2021. Cold-water coral habitat mapping: trends and developments in acquisition and processing methods. Geosciences 11 (1), 9. https://doi.org/10.3390/geosciences11010009.

Lo Iacono, C., Robert, K., Gonzalez-Villanueva, R., Gori, A., Gili, J.-M., Orejas, C., 2018. Predicting cold-water coral distribution in the Cap de Creus Canyon (NW Mediterranean): implications for marine conservation planning. Prog. Oceanogr. https://doi.org/10.1016/j.pocean.2018.02.012.

Loubrieu, B., Satra, C., 2010. Bathy-morphologie du plateau continental - façades Méditerranéenne et Corse (édition 2010, 100 m). Ifremer,Plouzané, p. In: Modèle bathymétrique (MNT) à 100m de résolution de la façade maritime française de la Méditerranée. Le MNT a été réalisé par krigeage à partir d'une compilation des principales sources de données bathymétriques françaises.

Lurton, X., 1998. Acoustique Sous-Marine, Ifremer ed. Ifremer, Brest. 1-114.

Maier, C., Bils, F., Weinbauer, M.G., Watremez, P., Peck, M.A., Gattuso, J.P., 2013. Respiration of Mediterranean cold-water corals is not affected by ocean acidification as projected for the end of the century. Biogeosciences 10 (8), 5671–5680. https://doi.org/10.5194/bg-10-5671-2013.

Makeev, A., Nikishkov, Y., Carpentier, P., Lee, E., Noel, J., 2010. Manufacturing issues and measurement techniques for assessment of the effects on structural performance of composite parts, in: American helicopter society international, I. In: American Helicopter Society 66th Annual Forum. American Helicopter Society International, Inc., Phoenix, AZ, pp. 11–13. May 2010.

Martín, J., Durrieu de Madron, X., Puig, P., Bourrin, F., Palanques, A., Houpert, L., Higueras, M., Sanchez-Vidal, A., Calafat, A.M., Canals, M., et al., 2013. Sediment transport along the Cap de Creus Canyon flank during a mild, wet winter. Biogeosciences 10 (5), 3221–3239. https://doi.org/10.5194/bg-10-3221-2013.

Matos, F.L., Company, J.B., Cunha, M.R., 2021. Mediterranean seascape suitability for Lophelia pertusa: living on the edge. Deep-Sea Res. Part I Oceanogr. Res. Pap. 170 https://doi.org/10.1016/j.dsr.2021.103496.

Mayer, L., Jakobsson, M., Allen, G., Dorschel, B., Falconer, R., Ferrini, V., Lamarche, G., Snaith, H., Weatherall, P., 2018. The nippon foundation-GEBCO seabed 2030 project: the quest to see the world's oceans completely mapped by 2030. Geosciences 8, 2. https://doi.org/10.3390/geosciences8020063.

Millot, C., 1990. The Gulf of lions' hydrodynamics. Continent. Shelf Res. 10 (9–11), 885–894. https://doi.org/10.1016/0278-4343(90)90065-T.

Millot, C., 1999. Circulation in the western Mediterranean Sea. J. Mar. Syst. 20 (1–4), 423–442.

Mouchi, V., Chapron, L., Peru, E., Pruski, A.M., Meistertzheim, A.L., Vetion, G., Galand, P.E., Lartaud, F., 2019. Long-term aquaria study suggests species-specific responses of two cold-water corals to macro-and microplastics exposure. Environ. Pollut. 253, 322–329. https://doi.org/10.1016/j.envpol.2019.07.024.

Mouchi, V., Vonlanthen, P., Verrecchia, E.P., Crowley, Q.G., 2017. Multi-scale crystallographic ordering in the cold-water coral Lophelia pertusa. Sci. Rep. 7 https://doi.org/10.1038/s41598-017-09344-5.

Ogston, A.S., Drexler, T.M., Puig, P., 2008. Sediment delivery, resuspension, and transport in two contrasting canyon environments in the southwest Gulf of Lions. Continent. Shelf Res. 28 (15), 2000–2016. https://doi.org/10.1016/j.csr.2008.02.012.

Orejas, C., Gori, A., Lo Iacono, C., Puig, P., Gili, J.M., Dale, M.R.T., 2009. Cold-water corals in the Cap de Creus canyon, northwestern Mediterranean: spatial distribution, density and anthropogenic impact. Mar. Ecol. Prog. Ser. 397, 37–51. https://doi.org/10.3354/mep08314.

Orejas, C., Kenchington, E., Rice, J., Kazanidis, G., Palialexis, A., Johnson, D., Gianni, M., Danovaro, R., Roberts, J.M., 2020. Towards a common approach to the assessment of the environmental status of deep-sea ecosystems in areas beyond national jurisdiction. Mar. Pol. 121 https://doi.org/10.1016/j.marpol.2020.104182.

Orejas, C., Wienberg, C., Titschack, J., Tamborrino, L., Freiwald, A., Hebbeln, D., 2021. Madrepora oculata forms large frameworks in hypoxic waters off Angola (SE Atlantic). Sci. Rep. 11 (1), 15170 https://doi.org/10.1038/s41598-021-94579-6.

OSPAR, 2010. Quality Status Report, Protection and Conservation of Biodiversity and Ecosystems. https://qsr2010.ospar.org/en/ch10_03.html.

Palanques, A., Durrieu de Madron, X., Puig, P., Fabres, J., Guillen, J., Calafat, A., Canals, M., Heussner, S., Bonnin, J., 2006. Suspended sediment fluxes and transport processes in the Gulf of Lions submarine canyons. The role of storms and dense water cascading. Mar. Geol. 234 (1–4), 43–61. https://doi.org/10.1016/j.margeo.2006.09.002.

Palanques, A., Puig, P., de Madron, X.D., Sanchez-Vidal, A., Pasqual, C., Martin, J., Calafat, A., Heussner, S., Canals, M., 2012. Sediment transport to the deep canyons and open-slope of the western Gulf of Lions during the 2006 intense cascading and open-sea convection period. Prog. Oceanogr. 106, 1–15. https://doi.org/10.1016/j.pocean.2012.05.002.

Pasqual, C., Sanchez-Vidal, A., Zuniga, D., Calafat, A., Canals, M., Durrieu de Madron, X., Puig, P., Heussner, S., Palanques, A., Delsaut, N., 2010. Flux and composition of settling particles across the continental margin of the Gulf of Lion: the role of dense shelf water cascading. Biogeosciences 7 (1), 217–231. https://doi.org/10.5194/bg-7-217-2010.

Paterson, G.L.J., Sykes, D., Faulwetter, S., Merck, R., Ahmed, F., Hawkins, L.E., Dinley, J., Ball, A.D., Arvanitidis, C., 2014. The pros and cons of using micro-computed tomography in gross and microanatomical assessments of polychaetous annelids. Mem. Mus. Vic. 71, 237–246. https://doi.org/10.24199/j.mmv.2014.71.18.

Pham, C.K., Ramirez-Llodra, E., Alt, C.H.S., Amaro, T., Bergmann, M., Canals, M., Company, J.B., Davies, J., Duineveld, G., Galgani, F., et al., 2014. Marine. Litter distribution and density in European seas, from the shelves to deep basins. PLoS One 9 (4), e95839. https://doi.org/10.1371/journal.pone.0095839 e95839.

Pires, D.O., Silva, J.C., Bastos, N.D., 2014. Reproduction of deep-sea reef-building corals from the southwestern Atlantic. Deep Sea Res. Part II Top. Stud. Oceanogr. 99, 51–63. https://doi.org/10.1016/j.dsr2.2013.07.008.

Poncelet, C., Billant, G., Corre, M.-P., 2020. Globe (Global Oceanographic Bathymetry Explorer) Software. https://doi.org/10.17882/70460. https://www.flotteoceanographique.fr/Nos-moyens/Logiciels-d-analyse/GLOBE/Telechargement.

Price, D.M., Robert, K., Callaway, A., Lo Iacono, C., Hall, R.A., Huvenne, V.A.I., 2019. Using 3D photogrammetry from ROV video to quantify cold-water coral reef structural complexity and investigate its influence on biodiversity and community assemblage. Coral Reefs. https://doi.org/10.1007/s00338-019-01827-3.

Puig, P., Canals, M., Company, J.B., Martin, J., Amblas, D., Lastras, G., Palanques, A., Calafat, A.M., 2012. Ploughing the deep sea floor. Nature 489 (7415), 286–289. https://doi.org/10.1038/nature11410.

Puig, P., Gili, J.-M., 2019. 27 submarine canyons in the mediterranean: a shelter for cold-water corals. In: Orejas, C., Jiménez, C. (Eds.), Mediterranean Cold-Water Corals: Past, Present and Future: Understanding the Deep-Sea Realms of Coral. Springer International Publishing, Cham, pp. 285–289. https://doi.org/10.1007/978-3-319-91608-8_27.

Puig, P., Palanques, A., Orange, D.L., Lastras, G., Canals, M., 2008. Dense shelf water cascades and sedimentary furrow formation in the Cap de Creus Canyon, northwestern Mediterranean Sea. Continent. Shelf Res. 28 (15), 2017–2030. https://doi.org/10.1016/j.csr.2008.05.002.

Rabineau, M., Berne, S., Aslanian, D., Olivet, J.L., Joseph, P., Guillocheau, F., Bourillet, J. F., Ledrezen, E., Granjeon, D., 2005. Sedimentary sequences in the Gulf of Lion: a record of 100,000 years climatic cycles. Mar. Petrol. Geol. 22 (6–7), 775–804. https://doi.org/10.1016/j.marpetgeo.2005.03.010.

Ragnarsson, S.Á., Burgos, J.M., Kutti, T., van den Beld, I., Egilsdóttir, H., Arnaud-Haond, S., Grehan, A., 2017. The impact of anthropogenic activity on cold-water corals. In: Rossi, S., Bramanti, L., Gori, A., Orejas, C. (Eds.), Marine Animal Forests: the Ecology of Benthic Biodiversity Hotspots. Springer International Publishing, Cham, pp. 989–1023. https://doi.org/10.1007/978-3-319-21012-4_27.

Raugel, E., Opderbecke, J., Fabri, M.C., Brignone, L., Rigaud, V., 2019. Operational and Scientific Capabilities of Ariane, Ifremer's Hybrid ROV, OCEANS 2019. Institute of Electrical and Electronics Engineers (IEEE), Marseille, France, p. 7. In: https://proceedings.oceans19mtsieeemarseille.org/session.cfm?sid=76.

Rawson, S.D., Maksimcuka, J., Withers, P.J., Cartmell, S.H., 2020. X-ray computed tomography in life sciences. BMC Biol. 18 (1), 21. https://doi.org/10.1186/s12915-020-0753-2.

Reid, M., Bordy, E.M., Taylor, W.L., le Roux, S.G., du Plessis, A., 2018. A micro X-ray computed tomography dataset of fossil echinoderms in an ancient obrution bed: a robust method for taphonomic and palaeoecologic analyses. GigaScience 8, 3. https://doi.org/10.1093/gigascience/giy156.

Reyss, D., 1964. Contribution à l'étude du rech Lacaze-Duthiers, vallée sous-marine des côtes du Roussillon. Vie Milieu 15 (1), 1–46.

Risk, M.J., Heikoop, J.M., Snow, M.G., Beukens, R., 2002. Lifespans and growth patterns of two deep-sea corals: *Primnoa resedaeformis* and *Desmophyllum cristagalli*. Hydrobiologia 471, 125–131. https://doi.org/10.1023/A:1016557405185.

Robert, K., Huvenne, V.A.I., Georgiopoulou, A., Jones, D.O.B., Marsh, L., Carter, G.D.O., Chaumillon, L., 2017. New approaches to high-resolution mapping of marine vertical structures. Sci. Rep. 7 https://doi.org/10.1038/s41598-017-09382-z.

Rogers, A.D., 1999. The biology of Lophelia pertusa (Linnaeus1758) and other deep-water reef-forming corals and impacts from human activities. Int. Rev. Hydrobiol. 84 (4), 315–406.

Sanchez-Vidal, A., Pasqual, C., Kerherve, P., Calafat, A., Heussner, S., Palanques, A., de Madron, X.D., Canals, M., Puig, P., 2008. Impact of dense shelf water cascading on the transfer of organic matter to the deep western Mediterranean basin. Geophys. Res. Lett. 35 (5), L05605 https://doi.org/10.1029/2007gl032825.

Sanchez-Vidal, A., Pasqual, C., Kerherve, P., Heussner, S., Calafat, A., Palanques, A., de Madron, X.D., Canals, M., Puig, P., 2009. Across margin export of organic matter by cascading events traced by stable isotopes, northwestern Mediterranean Sea. Limnol. Oceanogr. 54 (5), 1488–1500. https://doi.org/10.4319/lo.2009.54.5.1488.

Sanna, G., Freiwald, A., 2021. Deciphering the composite morphological diversity of Lophelia pertusa, a cosmopolitan deep-water ecosystem engineer. Ecosphere 12, 11. https://doi.org/10.1002/ecs2.3802.

Santin, A., Grinyo, J., Uriz, M.J., Lo Iacono, C., Gili, J.M., Puig, P., 2021. Mediterranean coral provinces as a sponge diversity reservoir: is there a mediterranean cold-water coral sponge fauna? Front. Mar. Sci. 8 https://doi.org/10.3389/fmars.2021.662899.

Savini, A., Marchese, F., Verdicchio, G., Vertino, A., 2016. Submarine slide topography and the distribution of vulnerable marine ecosystems: a case study in the Ionian Sea (eastern Mediterranean). In: Lamarche, G. (Ed.), Submarine Mass Movements and Their Consequences, 7th International Symposium. Springer, Nov. 2015, Wellington, New Zealand, pp. 163–170. https://doi.org/10.1007/978-3-319-20979-1.

Savini, A., Vertino, A., Marchese, F., Beuck, L., Freiwald, A., 2014. Mapping cold-water coral habitats at different scales within the northern ionian sea (central mediterranean): an assessment of coral coverage and associated vulnerability. PLoS One 9, 1. https://doi.org/10.1371/journal.pone.0087108.

Strömberg, S.M., Larsson, A.I., 2017. Larval behavior and longevity in the cold-water coral lophelia pertusa indicate potential for long distance dispersal. Front. Mar. Sci. 4 https://doi.org/10.3389/fmars.2017.00411.

Strömberg, S.M., Östman, C., Larsson, A.I., 2019. The cnidome and ultrastructural morphology of late planulae in Lophelia pertusa (Linnaeus, 1758)—with implications for settling competency. Acta Zool. 100 (4), 431–450. https://doi.org/10.1111/azo.12296.

Sultan, N., Gaudin, M., Berne, S., Canals, M., Urgeles, R., Lafuerza, S., 2007. Analysis of slope failures in submarine canyon heads: an example from the Gulf of Lions.

J. Geophy. Res. Earth Surf. 112 https://doi.org/10.1029/2005jf000408. F1, 0148-0227.

Taviani, M., Angeletti, L., Canese, S., Cannas, R., Cardone, F., Cau, A., Cau, A.B., Follesa, M.C., Marchese, F., Montagna, P., et al., 2017. The "Sardinian cold-water coral province" in the context of the Mediterranean coral ecosystems. Deep Sea Res. Part II Top. Stud. Oceanogr. 145 (Suppl. C), 61–78. https://doi.org/10.1016/j.dsr2.2015.12.008.

Taviani, M., Angeletti, L., Cardone, F., Montagna, P., Danovaro, R., 2019. A unique and threatened deep water coral-bivalve biotope new to the Mediterranean Sea offshore the Naples megalopolis. Sci. Rep. 9 https://doi.org/10.1038/s41598-019-39655-8.

Tubau, X., Canals, M., Lastras, G., Rayo, X., Rivera, J., Amblas, D., 2015. Marine litter on the floor of deep submarine canyons of the Northwestern Mediterranean Sea: the role of hydrodynamic processes. Prog. Oceanogr. 134, 379–403. https://doi.org/10.1016/j.pocean.2015.03.013.

Ulses, C., Estournel, C., Bonnin, J., de Madron, X.D., Marsaleix, P., 2008a. Impact of storms and dense water cascading on shelf-slope exchanges in the Gulf of Lion (NW Mediterranean). J. Geophy. Res. Oceans 113, C2. https://doi.org/10.1029/2006jc003795.

Ulses, C., Estournel, C., Durrieu de Madron, X., Palanques, A., 2008b. Suspended sediment transport in the Gulf of Lions (NW Mediterranean): impact of extreme storms and floods. Continent. Shelf Res. 28 (15), 2048–2070. https://doi.org/10.1016/j.csr.2008.01.015.

van den Beld, I.M.J., Bourillet, J.-F., Arnaud-Haond, S., de Chambure, L., Davies, J.S., Guillaumont, B., Olu, K., Menot, L., 2017. Cold-water coral habitats in submarine canyons of the Bay of Biscay. Front. Mar. Sci. 4, 118. https://doi.org/10.3389/fmars.2017.00118.

Vertino, A., Savini, A., Rosso, A., Di Geronimo, I., Mastrototaro, F., Sanfilippo, R., Gay, G., Etiope, G., 2010. Benthic habitat characterization and distribution from two representative sites of the deep-water SML Coral Province (Mediterranean). Deep-Sea Res. II 57 (5–6), 380–396. https://doi.org/10.1016/j.dsr2.2009.08.023.

Waller, R., Tyler, P., 2005. The reproductive biology of two deep-water, reef-building scleractinians from the NE Atlantic Ocean. Coral Reefs 24 (3), 514–522. https://doi.org/10.1007/s00338-005-0501-7.

Watremez, P., 2012. Canyon heads in the French Mediterranean Sea - overview of results from the MEDSEACAN and CORSEACAN campaigns (2008-2010). In: Wurtz, M. (Ed.), Mediterranean Submarine Canyons: Ecology and Governance. IUCN, Gland, Switzerland, pp. 105–112.

Wienberg, C., Titschack, J., 2017. In: [Rossi, S., Bramanti, L., Gori, A., Orejas, C. (Eds.), Framework-Forming Scleractinian Cold-Water Corals through Space and Time: A Late Quaternary North Atlantic Perspective, Marine Animal Forests: the Ecology of Benthic Biodiversity Hotspots. Springer International Publishing, Cham, pp. 699–732. https://doi.org/10.1007/978-3-319-21012-4_16.

Wolfl, A.C., Snaith, H., Amirebrahimi, S., Devey, C.W., Dorschel, B., Ferrini, V., Huvenne, V.A.I., Jakobsson, M., Jencks, J., Johnston, G., et al., 2019. Seafloor mapping - the challenge of a truly GLobal Ocean bathymetry. Front. Mar. Sci. 6 https://doi.org/10.3389/fmars.2019.00283.

Zibrowius, H., 1980. Les Scléractiniaires de la Méditerranée et de l'Atlantique nord-oriental, vol. 11. Mémoires de l'Institut Océanographique de Monaco, 1-238.